2023

STABILITY OF RUDDLESDEN-POPPER PHASE LANTHANUM NICKELATE AS AIR ELECTRODE FOR REVERSIBLE SOLID OXIDE CELLS

Daniel de Lorenzo Moreira
West Virginia University, dd00018@mix.wvu.edu

Stability of Ruddlesden-Popper phase Lanthanum Nickelate as air electrode for Reversible Solid Oxide Cells

Daniel de Lorenzo Moreira

Thesis submitted to

Benjamin M. Statler College of Engineering and Mineral Resources

At West Virginia University

In partial fulfillment of the requirements for the degree of

Master of Science in

Mechanical Engineering

Xingbo Liu, Ph.D., Chairperson

Wenyuan Li, Ph.D., Advisor

Wei Li, Ph.D.

Shanshan Hu, Ph.D.

Department of Mechanical and Aerospace Engineering

Morgantown, West Virginia

2023

Lanthanum Nickelate, Chromium, SOEC, SOFC, Long-term, Ruddelsden-Popper, EIS, DRT

ABSTRACT

Stability of Ruddlesden-Popper phase Lanthanum Nickelate as air electrode for Reversible Solid Oxide Cells

Daniel de Lorenzo Moreira

This thesis studied the long-term stability of Ruddlesden-Popper phase Lanthanum Nickelate under operating conditions as the air electrode for Reversible Solid Oxide Cells (R-SOC). Renewable energies have gone through an increase in popularity throughout the last decades, mainly due to the consequences of the rapid population growth in the world. These new energies have been pointed out as the rightful successor of fossil fuel energies in order to decrease the environmental impact of our day-to-day lives. Solid Oxide Fuel Cells as well as Solid Oxide Electrolysis Cells are believed to be the key to stabilizing the energy supply when environmental conditions are not favorable enough. In order to maximize operation efficiency and fulfill production needs, Solid Oxide Cells are arranged in stacks, in which metallic interconnectors provide support and connection from cell to cell. These interconnectors tend to segregate chromium-containing compounds at high temperatures, which leads to a rapid degradation of the cell and will likely end in cell malfunction.
Lanthanum Nickelate seems like a good electrode choice for this role due to its characteristics, both electrochemical and structural. Lanthanum Nickelate electrodes performed as air electrodes and were tested under chromium exposure and different conditions to simulate the effect that metallic interconnects would have on this air electrode material. The impact of chromium on the composition/structure and the performance of Lanthanum Nickelate were investigated in detail.

Both SOEC Anode and SOFC Cathode showed different behaviors under the exposure of external chromium sources throughout the 500 hours experiment span. The SOEC Anode showed a progressive degradation which could correlate with other studies. On the other hand, the SOFC Cathode did not suffer under exposure of chromium. The data that was collected from both sides was analyzed through DRT software to collect more information about what the electrochemical mechanisms look like at both electrodes.

The results showed that LNO would be a suitable option for Reversible Solid Oxide Cells in the future

ACKNOWLEDGMENTS

I would like to start by expressing my deepest gratitude to Dr. Xingbo Liu for providing me with the opportunity to pursue my degree and widen my understanding of the field.

I am thankful to Dr. Wenyuan Li for his wisdom, advice, understanding and patience during my research; not only when results were coming along, but especially when going through tough times.

I cannot forget about my coworkers and friends, who did not hesitate to help and support me when needed.

Special thanks to my family, who were always there for me and always had words of encouragement. None of this would have been achieved without them.

Finally, I want to thank my girlfriend Marta, for her encouragement and patience every single day.

LIST OF CONTENTS

LIST OF FIGURES ..... **vi**
1. INTRODUCTION **1**
1.1 SOLID OXIDE FUEL CELLS **2**
1.2 SOLID OXIDE ELECTROLYSIS CELLS **4**
1.3 REVERSIBLE SOLID OXIDE CELL **5**
1.4 BACKGROUND OF PREVIOUSLY USED MATERIALS **7**
1.5 RARE-EARTH NICKELATES **8**
1.6 RUDDLESDEN-POPPER PHASE RARE-EARTH NICKELATES **10**
1.7 RUDDLESDEN-POPPER PHASE LANTHANUM NICKELATE **11**
1.7.1 Catalytic Characteristics of Ruddlesden- Popper Phase Lanthanum Nickelate .. 12
1.7.2 Chemical Stability of RP-Phase LNO 13
1.7.3 Compatibility of LNO with GDC electrolyte 14
1.8 CHROMIUM POISONING **15**
2. EXPERIMENTAL METHOD **20**
2.1 CHARACTERIZATION **21**
2.1.1 XRD Analysis 21
2.1.2 EIS Analysis 21
2.1.3 SEM Observation 24
2.1.4 Distribution of Relaxation Times Deconvolution 24
2.2 CELL FABRICATION **24**
2.2.1 LNO Synthesis 24
2.2.2 GDC Electrode synthesis 25
2.2.3 Assembling of the cell 25
2.2.4 Chromium Source Synthesis 26
2.3 TESTING SET-UP **27**
3. RESULTS **28**
3.1- XRD **28**
3.2 LNO SINTERED AT DIFFERENT TEMPERATURES **29**
3.2.1-LNO sintered at 1000ºC. 29
3.2.2- LNO sintered at 1100ºC. 31
3.2.3- LNO sintered at 1200ºC. 32

3.2.4- LNO sintered at 1150ºC. 32
3.3- LONG STABILITY TESTING UNDER REGULAR AIR CONDITIONS 33
3.3.1- SOEC Anode mode 34
3.3.2- SOFC Cathode Mode 35
3.4- LONG TERM STABILITY TESTING UNDER CHROMIUM CONDITIONS 36
3.4.1- SOEC Anode 37
3.4.2- SOFC Cathode 38
3.4.3- Development of Polarization Resistances 39
3.5 SEM OBSERVATIONS 40
3.5.1 SEM figures of SOEC Anode under clean-air conditions 40
3.5.2 SEM figures of SOFC Cathode under clean-air conditions 41
3.5.3 SEM Figures of SOEC Anode under chromium exposure 41
3.5.4 SEM Figures of SOFC Cathode under Chromium exposure 41
3.5.5 EDX Spectroscopy 42
3.6 DRT DECONVOLUTION 42
3.6.1 SOEC Anode 43
3.6.3 SOFC Cathode 44
3.6.4 DRT deconvolution under different Po2 levels. 44
4. RESULTS ANALYSIS 46
4.1- EIS ANALYSIS UNDER CLEAN AIR 46
4.2- EIS ANALYSIS UNDER CHROMIUM EXPOSURE 47
4.3- SEM FIGURES 47
4.4- DRT DECONVOLUTION 48
5. CONCLUSION 51
6. BIBLIOGRAPHY 52

LIST OF FIGURES

Figure 1: SOEC vs PEM comparison by Versa Fuel Systems [42] 5
Figure 2: Scheme of a R-SOC. In this case, the electrolyte is a proton conducting electrolyte, therefore hydrogen protons will go through electrolyte and form water at the oxygen electrode [40]. 6
Figure 3: Perovskite-shaped REN in a ABO3 structure [39]. 8
Figure 4: Ruddlesden-Popper phase REN structure for n = 1, 2, 3 [39] 10
Figure 5: LNO/GDC symmetric cell 21
Figure 6: Example of Nyquist plot. The x-axis accounts for the real part of the impedance while the y-axis represents the imaginary part. R_s is ohmic resistance and $R_{electrode}$ represents polarization resistance [41]. 22
Figure 7: Gamry probes roles 23
Figure 8: 3-probe electrode set-up [41] 23
Figure 9: X-Ray Diffractometry of LNO. Reference PDF #11-0557. 28
Figure 10: Nyquist plot of LNO electrode sintered at 1000 ºC. Testing performed at 700 ºC. 29
Figure 11: SEM picture of the LNO-GDC interface. Testing perfrormed at 700 ºC 30
Figure 12: Nyquist plot of LNO electrode sintered at 1100 ºC. Testing performed at 700 ºC. 31
Figure 13: SEM picture of the LNO/GDC interface. LNO was sintered at 1100 ºC. 31
Figure 14: SEM pictures of the LNO/GDC interface. LNO was sintered at 1200 ºC 32
Figure 15: SEM pictures of the LNO/GDC interface. LNO was sintered at 1150 ºC. 32
Figure 16: Nyquist plot of LNO electrode sintered at 1150 ºC. Testing performed at 700ºC. 33
Figure 17: Nyquist plots of LNO performing as SOEC anode from (a) 0 to 72 (day 3) hours and (b) 96 (day 4) to 168 (day 7) hours. 34
Figure 18: EIS plots of LNO performing as SOEC anode from (a) 192 (day 8) to 264 (day 11) hours and (b) 288 (day 12) to 360 (day 15) hours. 34
Figure 19: EIS plots of LNO performing as SOEC anode from (a) 384 (day 16) hours to 456 (day 19) hours and (b) 480 (day 20) to 500 (day 21) hours. 34
Figure 20: EIS plots of LNO performing as SOFC cathode from (a) 0 to 72 hours (day 3) and (b) 96 (day 4) to 168 (day 7) hours. 35
Figure 21: EIS plots of LNO performing as SOFC cathode from (a) 192 (day 8) to 264 (day 11) hours and (b) 288 (day 12) to 336 (day 15) hours. 36
Figure 22: EIS plots of LNO performing as SOFC cathode from (a) 384 (day 16) to 456 (day 19) hours and (b) 480 (day 20) to 500 (day 21) hours 36
Figure 23: Nyquist plots of LNO in SOEC anode mode from (a) 0 to 72 (day 3) hours) and (b) 96 (day 4) to 168 (day 7) hours. 37
Figure 24: Nyquist plots of LNO in SOEC anode mode from (a) 192 (day 8) to 264 (day 11) hours and (b) 288 (day 12) to 360 (day 15) hours. 37
Figure 25: Nyquist plots of LNO in SOEC anode mode from (a) 384 (day 16) to 456 (day 19) hours and (b) 480 (day 20) to 500 (day 21) hours. 38
Figure 26: Nyquist plots of LNO in SOEC anode mode from (a) 0 to 72 (day 3) hours and (b) 96 (day 4) to 168 (day 7) hours. 38

Figure 27: Nyquist plots of LNO in SOEC anode mode from (a) 192 (day 8) to 264 (day 11) hours and (b) 288 (day 12) to 360 (day 15) hours. 39
Figure 28: Nyquist plots of LNO in SOEC anode mode from (a) 384 (day 16) to 456 (day 19) hours and (b) 480 (day 20) to 500 (day 21) hours. 39
Figure 29: Polarization Resistance under (a) clean-air conditions and (b) chromium exposure. 40
Figure 30: SEM Figures of SOEC Anode exposed to clean air conditions for 500 hours at different magnitudes (a) and (b). In picture (a) the GDC layer is seen on the bottom part of the image while GDC is located on the left side of picture (b) 40
Figure 31: EM Figures of SOFC Cathode exposed to clean air conditions for 500 hours at different magnitudes. In pictures (a) and (b), the GDC electrolyte is located on the left of the image. 41
Figure 32: SEM Figures of SOEC Anode exposed to chromium conditions for 500 hours at different magnitudes. Figure (a) focuses on the GDC-LNO interface. Figure (b) zooms in to focus on the LNO electrode in order to get a better image of the grains. Figure (c) shows an increased zoom on the LNO-GDC interface 41
Figure 33: SEM Figures of SOFC Cathode under chromium exposure for 500 hours at different magnitudes. Pictures (a) and (b) focus on the GDC-LNO interface at different but similar magnitudes. Picture (c) focuses on the LNO grain size. 41
Figure 34: EDX Spectroscopy of (a) SOEC Anode and (b) SOFC Cathode after long-term testing under chromium exposure. Red plot represents the electrode before operation. 42
Figure 35: (a) and (b) show the DRT deconvolution of the SOEC Anode side at 0 and 21 days respectively. (c) and (d) correspond to the SOEC Anode side performing under chromium exposure at 0 and 21 days. 43
Figure 36: (a) and (b) show the DRT deconvolution of the SOFC Cathode side at 0 and 21 days respectively. (c) and (d) correspond to the SOFC Cathode side performing under chromium exposure at 0 and 21 days 44
Figure 37: DRT deconvolution of the LNO electrode at 0 hours under (a) regular air and (b) 40% P_{O2} 44

1. INTRODUCTION

According to the United Nations, the world's population is more than three times larger today than it was halfway through the twentieth century. On top of that, the global human population reached 8 billion people in November 2022, adding 1 billion since 2010 and 2 billion since 1998. Therefore, this growth has accelerated the process of globalization that humankind has been going through since the Industrial Revolution. This process of globalization can be interpreted as the phenomenon that explains the increasing cultural, technological, and economic interdependence that people from all over the world are going through in their everyday lives.

The demand and supply of resources are also going through the same globalization phenomenon. Resources are exported and imported from different countries based on citizens' needs. At the center of all these processes is energy, which can be seen as both a resource and a way to achieve them. Energy is needed in all parts of our routines nowadays, from cooking our food, working, or heating our homes. No matter what we do, electrical energy is behind all those processes.

In the 18th century, the steam engine was invented. By burning a fuel, which used to be coal (fossil fuel), water is boiled, and high-pressure steam is released into a cylinder, which causes the piston to move and generate the needed movement or displacement. After that, fossil fuels were established as a high-demand resource, thanks to the acceleration of processes. We see how coal, natural gas, and petrol are pivotal in the world. Most of the energy that was generated before the surge of renewable energies was generated through the burning of these fuels. However, the cons of using these resources should have been considered when they burst into the scene. Later, when technological developments and studies were completed, it was possible to measure how much damage had already been done. On top of polluting the air, these gases favored the "greenhouse effect." This phenomenon lets the heat and light generated from the sun come through the atmosphere but does not let the thermic waves get out of it, causing a block that makes them bounce back towards Earth, with a consequent constant increase in global temperature.

As a response to the greenhouse effect, renewable energies were born. These alternative ways to generate energy were based on the atmospheric conditions of the location.

Eolic and solar energy used existing resources that depended on the weather. Nevertheless, the main issue with these energies was consistency. The wind is not constantly blowing, and the sun is not shining at its brightest when it is cloudy. This is where Solid Oxide Cells (SOC) come into play. These electrochemical devices take fuel as an input, generating electricity as an output. This process occurs due to a series of Red-Ox reactions inside the cell. Opposite to a battery, in which the electricity is limited, a fuel cell will keep generating electricity as long as fuel is provided.

On the other hand, some cells could revert the process and generate fuel (hydrogen in this case) by being used as an electrolysis cell (SOEC). Through this, atmospheric conditions would no longer compromise the energy supply. The cell would then aid the alternative energy source when there are no conditions for it, such as lights wind currents for wind turbines, or not enough bright light for the solar panels to supply the desired electricity input. On the other side, the cell would work as a water splitter to store hydrogen when the windmill or solar panel can generate enough to supply the demand. Therefore, this fuel would be used when atmospheric conditions are not favorable enough to resupply a target input.

1.1 SOLID OXIDE FUEL CELLS

As stated before, there are different types of SOCs. Solid Oxide Fuel Cells (SOFCs) might be the most known ones and are a part of the focus of this study. SOFCs transform the chemical energy that the fuel stores into electrical energy through chemical reactions. The Red-Ox reaction that happens within the cell can be split into the following reactions [21]:

1. $H_2 + O^{2-} \rightarrow H_2O + 2\,e^-$

2. $\frac{1}{2}O_2 + 2e^- \rightarrow O^{2-}$

Formula 1: Hydrogen and oxygen molecules bind together to form water plus the release of two electrons.

Formula 2: Oxygen Reduction Reaction (ORR)

The process of generating electricity through a fuel cell can be simplified into four steps: delivery of reactant, electrochemical reaction, ion conduction, and byproduct removal [21]. The device must have an uninterrupted fuel supply to produce electricity, and it always demands a fast and efficient reactant supply. Following this, hydrogen is delivered to the anode (also referred to as the hydrogen electrode), while oxygen is delivered to the cathode (oxygen electrode). The reactant supply is the jumpstart event that will start the chain effect throughout the cell, and the efficiency of the process is seen as crucial for the overall performance of the device. This delivery process is generally provided using flow field plates. These plates consist of tiny channels that provide a homogeneous distribution to the porous electrode to ensure that the whole reaction surface will generate an equal or at least similar reaction rate. Once the reactant has been delivered to the electrodes, they undergo their respective electrochemical reactions. The current that is generated in the reaction is proportional to both the speed of the reaction and the reaction surface area. A fast electrochemical reaction will generate a higher current output, which is the primary goal.

The reaction involves a transfer of energy from the fuel to the electrons to create the current. The transfer is finite and must occur at the electrolyte/electrode interface, or the triple-phase boundary if a barrier layer is needed. Therefore, a more extensive interface will provide a larger space for the reaction to happen. Hydrogen is oxidized at the anode, while oxygen is reduced at the cathode. Although particles will be displaced from one side of the cell to the other end, the charge balance of the reaction must stay neutral. Both ions and electrons go through their transportation channels to the other side of the electrolyte between the electrodes. The way electrons follow to get to the cathode is relatively easy since it consists of an external path that can go from anode to cathode. However, ionic transport is more complex than that since ions must flow through the electrolyte. The ion transport mechanism consists of moving from one vacancy to another, with lots of them being lost when going through a phase change, lowering the efficiency of the process. This results in resistance loss and lower cell performance. Since ions must go through the whole thickness of the electrolyte, the solution is to have a thinner electrolyte, shortening the path of the ions and therefore reducing the ionic loss. However, due to its thinner structure, this electrolyte is incapable of providing the mechanical strength that is typically provided by its thicker

version. In this case, the cell is mechanically supported by a thicker anode, which also allows for a larger surface area in which the fuel can go through the oxidation reaction.

Like in any reaction, unwanted byproducts must be removed or will build up over time, preventing reactants from reacting. The mechanisms that are responsible for the transportation of reactants into the cell tend to be the same as the ones that are used to evacuate byproducts, even being the same channels at times.

1.2 SOLID OXIDE ELECTROLYSIS CELLS

The needed components for an operational electrolysis cell are the same ones that are needed for a fuel cell: two electrodes (anode and cathode) and an electrolyte. Electrolysis cells also follow 4 steps trough their process, same as a fuel cell, although their order is reversed. The reactions in a SOEC go as follows:

$$3.\ O^{2-} \rightarrow \frac{1}{2}O_2 + 2\,e^-$$

$$4.\ H_2O + 2\,e^- \rightarrow H_2 + O^{2-}$$

Formula 3: Oxygen Evolution Reaction (OER)
Formula 4: Water Splitting Reaction

In the electrolysis process, steam is delivered to the anode, where it will go through a water splitting reaction. As the name of the reaction points, water is split into hydrogen and oxygen. Hydrogen gas is then evacuated from the cell while oxygen ions (negatively charged) go through the electrolyte towards the cathode. In the anode, oxygen ions will go through a transformation into oxygen molecules through an oxygen evolution reaction (OER) [8].

The hydrogen that is produced during the reaction is then stored and used as fuel in SOFCs when external energy sources do not meet supply demands. The main advantage of SOECs concerning other electrolysis methods (such as Polymer Electrolyte Membrane Cells) is a higher efficiency and lower cost due to a lesser amount of electricity and noble metal catalysts required. According to Versa Power Systems, SOECs can achieve a three to four times larger hydrogen production in the range of 45 to 50 Wh/g. The following plot shows

the comparison between both devices following the results of the previously mentioned fuel cell company:

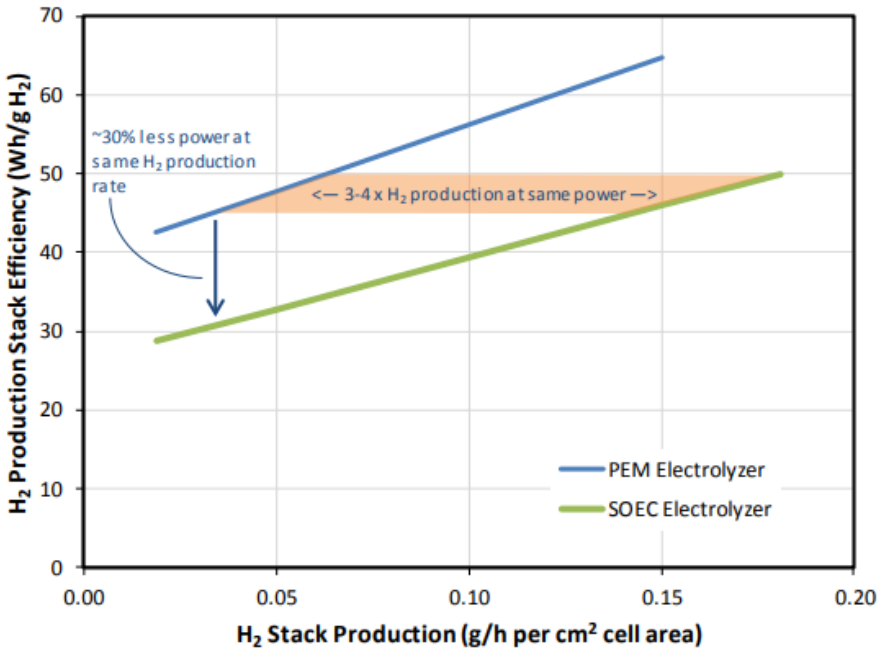

Figure 1: SOEC vs PEM comparison by Versa Fuel Systems [42]

The difference in efficiency between both devices is mainly caused by the temperature increase needed to operate a SOEC which typically stays above 700 ºC. This operating temperature no longer needs a significant electric supply, as it is traded for the thermal energy that is present at this point of the process. Furthermore, these high temperatures also speed up the reaction kinetics, leading to a decrease in internal cell resistance and a consequent increase in efficiency.

1.3 REVERSIBLE SOLID OXIDE CELL

An ideal cell set-up would be one in which both electrodes could offer a high-efficiency performance when the cell is performing as SOFC or SOEC. In that case, the implementation of Reversible Solid Oxide Cells (R-SOCs) would make the extension and commercialization of the cells easier, as only one cell would be needed instead of one SOFC

and one SOEC. R-SOCs are a specific type of cell that can work as any of the previously mentioned cells by reversing the way the current goes through the cell.

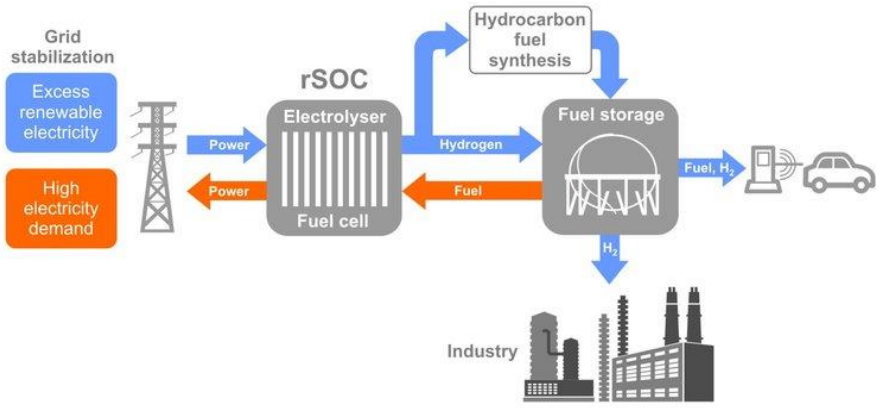

Figure 2: Scheme of a R-SOC. In this case, the electrolyte is a proton conducting electrolyte, therefore hydrogen protons will go through electrolyte and form water at the oxygen electrode [40].

When working as a fuel cell, fuel and oxygen would have to be provided through the anode and cathode, respectively, promoting the reactions throughout the cell, with current flowing from the anode to the cathode. On the other hand, when working as an electrolysis cell, water would have to be supplied through the cathode, and current would run the other way around, flowing from what would be the SOFC cathode, now working as a SOEC anode.

Like any other energy-related issue, R-SOCs also show some issues that could be solved with current ongoing research. One of them is the limited commercialization found nowadays, partly due to the early stages of technology, which means there needs to be more experience in the large-scale implementation and operation of RSOC systems. Another is finding suitable materials with high performance in electrolysis and fuel cell modes. On top of that, these materials must show an excellent price-performance ratio if this technology wants to grow exponentially, as it will be needed in years to come.

As previous studies show, the implementation and extensive commercialization of R-SOCs would be the ideal situation in the future. The efficiency of R-SOCs varies depending on the design and operating conditions but are known to have high efficiency in both modes, especially when compared to combustion processes. The electrical efficiency of

these electrolysis devices is measured as a percentage of the actual energy that is used in the reaction over the theoretical energy required for the reaction to happen. These measurements on R-SOCs when performing in fuel cell modes range from 50% to 60% when talking about electrical efficiency. However, it shows an estimate of up to 90% when waste heat is recovered and used as a thermal energy source. In electrolysis mode, R-SOCs typically range between 50% to 80% [4]; usually depending on the source of the electricity used to power the reaction. That is a significant difference when comparing numbers with traditional fossil fuels. Coal-fired power plants typically range from 33% to 48%, while natural gas power plants can range from 42% to 60%. Due to all the developments and promising results that R-SOCs have shown, they present themselves as a perfect candidate to establish grid stabilization through renewable energies.

1.4 BACKGROUND OF PREVIOUSLY USED MATERIALS

Before rare-earth nickelates were postulated as prospective materials for SOFC cathodes, state-of-the-art materials such as lanthanum strontium manganites ($La_{1-x}Sr_xMnO_3$) and lanthanum strontium ferrites ($La_xSr_{1-x}Co_yFe_{1-y}O_{3-\delta}$) were the materials that were predominantly used as oxygen electrodes. The main problem behind using these materials is their reactivity towards chromium, which, on the other hand, is the main strength behind the materials that were analyzed in this thesis.

The reactivity of LSM towards chromium becomes an issue when operating at high temperatures [3]. Chromium at temperatures above 600 ºC can be highly volatile and can cause the formation of vacancies in the lattice that will finally lead to compromising the performance and stability of the electrode. Wang [29] tested two different composite cathodes, one of them being a composite cathode LSM-GDC. When observing the material's behavior after exposure to chromium, it was seen that the chromium's deposition was located at the electrolyte/cathode interface after a galvanostatic operation, affecting the reaction area. This deposition was attributed to the presence of manganese in the compound, which caused a rapid degradation of the material.

LSCF is another material that has been widely used as oxygen electrode for SOFCs. Bentzen [3] tested an LSCF-CGO composite cathode and compared it to the behavior of

LSM-YSZ. In his analysis, the LSCF composite showed a lower degradation than that of the LSM composite, which correlates with the big degradation that Wang [29] saw in the compound. Although the LSCF does not get to the extent of the LSM compound in terms of degradation, the damage that chromium inflicts on LSCF is too significant to conclude that the material is valid for long-term operation.

1.5 RARE-EARTH NICKELATES

In this study, rare-earth nickelates (REN) were used as a material for both SOEC anode and SOFC cathode. Although a specific group within REN was used in this experiment (Ruddlesden-Popper phases), some general background about REN is needed to explain the characteristics of these compounds. REN have been used in SOFC applications since the late 1990s when developments in deposition techniques allowed the formation of high-quality films of these materials.

REN have different properties that make them excellent candidates for R-SOCs applications to those of previously mentioned LSCF and LSM. REN commonly show a perovskite-like ABO_3 [2] configuration in which B is a 3d transition metal (nickel) and A corresponds to a rare-earth material (A = lanthanum, praseodymium, neodymium, samarium…etc..). The crystal structure of a perovskite-shaped REN is shown in the following figure:

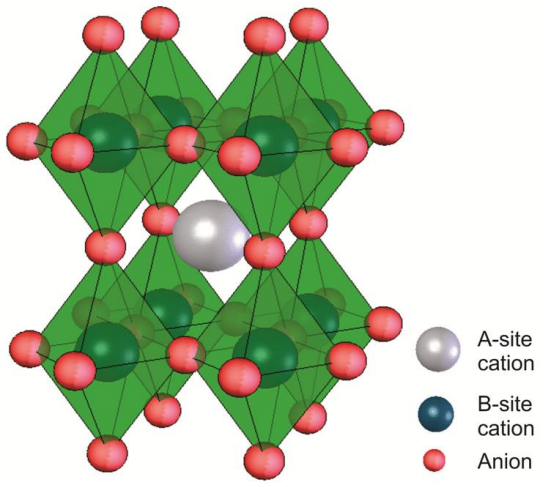

Figure 3: Perovskite-shaped REN in a ABO3 structure [39].

From an electronic point of view, REN show a metal-insulator transition (MIT) [38] seen when exposed to changes in external conditions, especially temperature and oxygen partial pressure. When cooled or heated, REN changes from a metallic state to an insulating state, respectively. This causes the material to behave like a metal, where the electron's bonds within the atoms are not tight enough, tending to move quickly and showing a more significant degree of freedom. On the contrary, insulation states show their respective properties because of how tightly bound electrons are to their atomic nucleus, being incapable of moving. Furthermore, by tuning external temperature, a high electronic conductivity can be influenced on the material to cause an efficient transference of electrons; promoting a better and more efficient oxygen reduction reaction. This allows for a higher cell performance and a decrease in polarization losses.

There are multiple characteristics that qualify REN as valid materials for air electrodes in R-SOCs, to the detriment of manganites and ferrites. REN tend to have longer lifespans due to the difference in operating temperature ranges that both materials move within. Due to its low ionic conductivity, LSM cannot offer a high-efficiency output when operating in the intermediate temperature (600ºC -800ºC) range that REN tend to operate in. Furthermore, decreasing the operating temperature allows REN to avoid changes in the initial crystal structure, leading to stable and efficient performances at said temperatures. But the pivotal characteristic that REN show is their chemical stability when exposed to poisoning agents that will appear throughout operation, such as chromium-containing compounds. This is partly due to the difference in the crystal structure, which allows for a stable environment for the nickel cations. On top of that, the oxidation state of the nickel cations that occupy the B-site in REN seem to be more stable when compared to the manganese cations that occupy the same site in LSM.

All these characteristics allow for faster reaction rates and better oxygen-ion diffusion reactions on the surface or through the bulk. A degradation in the oxygen-ion diffusion mechanism would most likely end in a rapid degradation of the cell and finally, an operating failure.

1.6 RUDDLESDEN-POPPER PHASE RARE-EARTH NICKELATES

Within the group of Rare-Earth Nickelates, there is a specific alteration in the atomic structure which shows an enhanced performance in the applications of SOC. This is the group of Ruddlesden-Popper (RP) Phase REN. These materials are considered great alternatives to traditional REN because of their superior mixed ionic and electronic conductivities, dielectric properties, and mainly for their capacity to incorporate excess oxygen ions into the lattice, which enhances the oxygen diffusion due to a higher bulk diffusivity [20, 1]. This last characteristic is why this compound has been targeted as the only material to be used in this experiment. The configuration of RP phases shows a structure in which a number of "n" perovskite layers are stacked between AO rock-salt layers along the c-axis. The rare-earth element (commonly A= La, Nd, Pr) occupies the A-site, while a transition or post-transition metal is at the B-site (nickel in this case). The next figure portrays the structure of a Ruddlesden-Popper phase rare-earth nickelate:

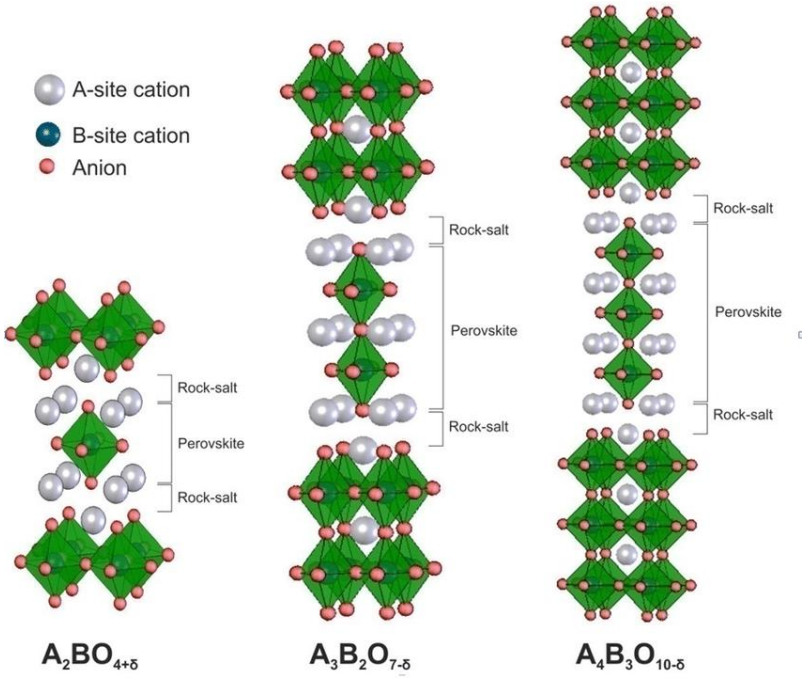

Figure 4: Ruddlesden-Popper phase REN structure for n = 1, 2, 3 [39]

As stated before, the main difference between RP phases lies within the oxygen transport properties. These materials can become hypo-stoichiometric (less than stoichiometric compound) in higher-order RP phases or hyper-stoichiometric (more than stoichiometric compound) in lower-order RP phases such as the one that was used in this experiment. This reflects the different oxygen ranges that RP phases can move within. The reason behind this lies in the interstitial sites that the structure provides, which create alternative, although necessary, pathways for oxide ion migration via hopping from one interstitial site to another.

These RP phases can be modified and doped with other materials, like any other compound, in order to enhance their characteristics. RP phases can go through doping of the A-site or B-site element, which can alter the structure of the compound. Commonly, this doping is used to create angle distortions between sites, giving birth to new oxygen ion vacancies, which could help the oxygen diffusion mechanism.

1.7 RUDDLESDEN-POPPER PHASE LANTHANUM NICKELATE

Ruddlesden-Popper phase Lanthanum Nickelate (following LNO) was the chosen material for this experiment. The behavior of LNO shifts from a semiconductor behavior when n = 1 to a metallic behavior at n > 1. LNO shows the alternated $LaNiO_3$ /rock-salt LaO layer distribution that distinguishes RP phases, also sharing the same characteristics as previously named RP phases but showing differences with other commonly used RP phase nickelates [15] (Neodymium, Praseodymium).

LNO´s electronic behavior is distinguished by electron-electron interactions. This can be explained by the partially filled 3d electron layer in the nickel atoms, causing electrons to be prone to interact with each other. This leads to the aforementioned enhanced electronic conductivity of the material.

Due to different synthesis methods and oxygen partial pressures, LNO shows a variable oxygen stoichiometry and results in the creation of different $La_2NiO_{4+\delta}$ phases. The oxygen stoichiometry in LNO tends to show an over-stoichiometry in the compound, which is induced by the incorporation of oxygen ions into interstitial sites within the LaO rock-salt layer. As stated before, this improves the oxygen ion diffusion within the electrode, as the

bulk diffusivity is enhanced due to the modification of both crystal symmetry and lattice parameters. On top of that, when oxygen ions are present in the lattice at high interstitial concentrations, the NiO_6 octahedra is prevented from tilting, preserving the symmetry in the unit cell and leading to phase stabilization.

1.7.1 Catalytic Characteristics of Ruddlesden- Popper Phase Lanthanum Nickelate

Although the specific structure that this study is focused on is $La_2NiO_{4+\delta}$, this corresponds to the first order of the structure $La_{n+1}NiO_{3n+1+\delta}$. Therefore, there are multiple compounds that follow at n > 1. LNO is a great candidate as a high-efficiency, cost-effective electrocatalyst, mainly due to the great intrinsic oxygen evolution and oxygen reduction reaction kinetics that it shows.

Precious metal electrocatalysts have been identified as excellent oxygen electrode catalysts. Platinum is known to be a great catalyst for ORR in SOFC cathodes, while iridium is used to promote OER in SOEC anodes. The main issue with these materials is the high cost, added to their low bifunctionality and inability to replicate the same efficiencies in their counterparts' reactions. Therefore, by being unable to be used in both reactions, the cost of achieving a high efficiency on both sides of the cell adds up and makes their worldwide commercialization more difficult.

As stated before, RP phase LNO could solve this problem due to the excellent kinetics that it shows during ORR and OER. Choi [7] reports that the n-value (number of perovskite layers) influences the electrocatalytic properties of LNO, as well as their ability to store excess interstitial oxygen due to the higher number of interstitial sites between perovskite ($LaNiO_3$) and rock-salt (LaO) layers. Following this study, Choi concludes that higher-order RP phase LNO show excellent bifunctional catalytic properties, being linearly progressive with the order of the n-value of the compound. On top of that, the stability of L5N4 was tested in a durability test and only showed a 6mV potential decrease after 1000 cycles acting as a catalyst in OER, which shows the high chemical stability of the compound during OER. L5N4 was also tested for 10,000 cycles as a catalyst for ORR and showed a decline of 37 mV.

Choi [7] also reports that through the use of glycine-nitrate combustion (GNC) and an adaptation of the fuel-to-oxidizer ratio in the combustion to an extremely fuel-abundant atmosphere, the 4 layered perovskite LNO can be synthesized as a single RP phase with transition metal dopants in the compound. The addition of dopants such as cobalt in this case enhances the catalytic performance of the compound due to a higher oxidation state in Ni.

1.7.2 Chemical Stability of RP-Phase LNO

The matter of R-SOC as a reliable conversion of energy to sustain a renewable-energy-based society is a matter of long operating cycles. To achieve an efficient and reliable energy supply, the cell must be both electrochemically and chemically stable, especially due to the temperatures that R-SOC will be operating at.

Cebasek [5] tested the chemical decomposition of LNO at a high temperature for 800 hours and saw that LNO can go through decomposition into La_2O_3 and NiO when going through an oxygen partial pressure gradient. When exposed to a high P_{o2}, NiO particles were formed, while side pores were created at the low P_{o2} side. La_2O_3 impurities were not seen at the latter site, although it was believed to remain within grain boundaries.

When exposed to dry air, LNO is stable in a wide range of T- P_{o2} conditions when they are constrained as isobaric and isothermal, respectively. Pilaklova [24] reflects on it when also stating that other nickelate phases at n = 2, 3, or infinite are thermodynamically more favorable at temperatures below 900ºC. Phase transformations from $La_2NiO_{4+\delta}$ into higher-order RP phases or perovskite-structured $LaNiO_3$ are known to be suppressed, although a higher-order transformation can happen in the long term. Amow [1] detected a secondary phase which could be a higher order RP phase (n = 2) after sintering the sample in air at 900ºC for 2 hours. This transition into a higher-order RP compound is accompanied by a slow increase in overall electrical conductivity with time. Therefore, Pilaklova concludes that RP phase LNO tends to be thermodynamically stable at T > 1200ºC and shows a metastable behavior at T < 900ºC. Under Schrödl's [26] findings, there is a discrepancy over how and where LNO decomposes. Although there were other formed compounds in the findings (due to external factors that will be neglected for the purpose of this study), LNO shows good overall stability under dry air. However, the external layer of LNO showed some lanthanum

across the surface, which is believed to have migrated from within the bulk region, as well as NiO inclusion along the grain boundaries of LNO.

1.7.3 Compatibility of LNO with GDC electrolyte

Gadolinium doped ceria (GDC) was the chosen electrolyte material in this experiment. The characteristics of GDC will be reviewed in this section as well as the chemical, electrochemical and mechanical compatibility with LNO.

The electrolyte is one of the critical parts in the cell, as it will separate both electrodes and prevent both reactions from merging, assigning one side of the layer to each of them. High ionic conductivity is desired for the operation of these electrolytes, and ceria-based materials (especially GDC) are perfect candidates due to their ion conduction characteristics. Ohmic losses commonly happen due to poor oxygen ion transport through the electrolyte. These contribute to the cell's overall performance by not letting oxygen ions go through and complete the cell's cycle. These losses can add up with respective polarization losses in the electrodes, partly due to the difficulty of oxygen ions when going through the electrolyte. Therefore, the role of the electrolyte must not be overlooked, as it will clearly contribute to poor cell performance and low efficiency. Since the oxygen ions must go through the whole electrolyte thickness through hopping mechanisms, ohmic losses are linearly proportional to the thickness of the layer.

Furthermore, anode-supported cells are based on that principle: the anode becomes thicker to give the cell some mechanical strength and let the electrolyte become thinner, making it less complicated for ions to hop through it and reduce overall losses throughout the cell. On the other hand, when building symmetric cells, the main components that want to be tested are the electrodes based on their own reactions without trying to achieve a whole cell cycle. Therefore, the electrolyte becomes thicker than in anode-supported cells, giving mechanical support to the cell and ensuring that electrodes will not be damaged in the handling and operation of the cell.

One of the main concerns when working with GDC is the need for more research on an ideal sintering temperature. Reports in the literature have yet to be consistent on the progression of the density of the material based on its sintering temperature. Yasuda [31]

found some pores form in the range of 1300ºC -1400ºC. At the same time, it was found that 1200ºC had the best relative density achieving a relative density of roughly 98% while showing a 3% decrease down to 95% after sintering at 1400ºC. This fact could not be explained at the moment of the study, as the total mass loss after sintering was 1%, which should not have been accountable for the decrease in density. Following previous data, the mechanical properties when increasing the sintering temperature above 1200ºC were affected. Both Young's modulus and fracture strength decreased, which can be explained by the formation of previously mentioned pores in the structure. The experimental part will mention and explain the temperature used in this experiment.

When reviewing the behavior of LNO electrodes on GDC electrolytes, both tend to be compatible with each other and show no reactivity signs with one another. Reports of both half and full cells have been found in which GDC is the chosen electrolyte for LNO to be applied on. On top of that, GDC can act as a diffusion barrier layer when REN are applied on commonly used yttria-stabilized zirconia (YSZ) electrolytes, a material that is known to be highly reactive in the presence of lanthanum.

1.8 CHROMIUM POISONING

In order to maximize cell performance and output results, cells tend to be connected in stacks using interconnects. This allows cells to perform in series and meet the voltage and power density required to perform in large-scale applications. These interconnects also work as a mass transport channel to provide fuel and air to the cell while acting as evacuation exits. The mass transport function allows the cell to eliminate any excess and undesired byproducts that would prevent it from performing at the highest possible performance. The latter function states the main reason behind the interconnectors: to provide a connection between cells that would add the individual voltages of all the cells within the stack.

Within cell interconnectors, ceramics and metals tend to be widely used materials, partly due to their mechanical and thermal expansive characteristics. Ceramic materials were the first ones to be used as interconnectors for large-scale applications of SOFCs [21]. These materials would provide mechanical strength to the stack to prevent the individual cells from suffering any external or internal damage. Any external damage could be inflicted on the cells during the handling or installation of the stack that could cause internal damage. On the

other hand, the high temperatures that fuel cells tend to be exposed to during operation could create a thermal expansion that could damage any component within the cell if thermal expansion coefficients do not have similar values, or if the rate of the electrochemical reactions happening at the triple phase boundary does not happen as predicted, causing tensile strength within the cell that could finally lead to delamination on the long-run. The downside of ceramic interconnectors is the low electrical conductivity of these materials. This results in low cell performance, as it would mean that there would be electrical current losses since some of it would be lost before reaching the end of the stack. To improve a stack's electrical conductivity, metallic interconnectors (MIC) were implemented. Metallic materials [35] would keep providing the mechanical support and dual atmosphere that ceramics were providing while improving the electrical current flow needed for optimal stack performance.

Metallic materials would result in a higher electronic and thermal conductivity, a lower cost, and a more straightforward fabrication, which would lead to a decrease in the stack's overall production cost, also favoring the expansion of large-scale commercialization. The thermal characteristics of MICs also help decrease the SOFCs operating temperature from a high-temperature range (800ºC -1000ºC) to an intermediate range (600ºC -800ºC). MICs are typically alloys that contain aluminum, silicon, or chromium that form a semi-conductive scale on the surface of the alloy when in the presence of oxygen (oxygen that would flow into the cathode to go through ORR). This protective layer will reduce Cr, Al, or Si evaporation and diffusion into the cell when operating within high-temperature ranges. All these mentioned elements show excellent oxidation resistance, but Cr is the one that shows the best electrical conductivity in the long run. Compared to other materials, the enhanced electrical conductivity decreases the possibility of having ohmic losses in the cell.

The main downside to chromium is the changes in the alloy's structure at the alloy-scale interface. Porous layers will form due to these structural changes, leading to a continuous "emptying" of the layer that will eventually lead to a lower bonding between particles and a decrease in the densification of the structure. Combined with the stress that stacks go through during operation, chromium scales can show delamination and, eventually end in cell failure due to poor connection or total loss of it. Besides the mechanical changes that the cracking of the chromium scale can inflict on the cell, it can also alter its behavior and electrochemical performance. It has been studied that gaseous compounds can evaporate

from the scale layer and end up in the cathode, where the ORR will occur. The previously mentioned chromia scale that is formed on the surface of the alloy is known to be Cr_2O_3 [35,34]. However, various gaseous species tend to form under different operating conditions and cell-contained materials. Factors such as temperature, air humidity, flow rate, or polarization can determine the compound that will be formed, which is explained by the abundance or absence of oxygen and hydrogen in the atmosphere. Regarding the matter of humidity, chromium oxyhydroxide ($CrO_2(OH)_2$) tends to be the predominant compound, while chromium oxide (VI) (CrO_3) is seen in dryer conditions. As temperature increases, other compounds form, predominantly $CrO_2(OH)_2$ and chromium oxide (CrO_3) [34].

Flow rate is seen as another critical factor when exposing SOCs to chromium. Following previous studies, a low flow rate will lead to higher species concentration in the gas. On the other hand, a high flow rate results in a lower concentration in short-term studies but can add up to a higher total amount of chromium in the long run.

One of the critical external factors when talking about cell efficiency and performance is the cell's behavior when exposed to external polarization, which is one of the main aspects of the cell's operating process. How the cell behaves when applying an external current can give a hint about what the overall resistance of the cell will be during operation, as well as how the electrochemical reactions will take place if it is the case of an SOEC or R-SOC. Again, the electrode's performance will be different depending on the material and the quantity of Cr that will be deposited on it. The performance of state-of-the-art lanthanum strontium manganate (LSM) under polarization in the presence of chromium sources was previously studied, as well as lanthanum strontium chlorite ferrite (LSCF) and newer materials such as lanthanum nickelate ferrite (LNF) [29]. As can be seen, all these compounds have a rare-earth material in them, lanthanum in this case. This highlights the development of compounds with their A-site occupied by a rare-earth material. From LSM studies, it is seen that the amount of chromium that can be found in the cathode and its correspondent polarization loss is more significant when a current density of 300 mAcm^{-2} (ideal current density) is larger than the ones that are found when no current is applied to the cell under open circuit conditions. Therefore, polarization plays a big part in the long-run degradation of the cell, not only because of the operation degradation but also because of how it affects the response of the cell to external contamination such as chromium exposure.

This study focuses on the long-term stability behavior of R-SOC air electrode LNO cells when exposed to a chromium source, replicating the presence of the chromia scale that would form in the presence of a MIC. In previous studies, the ability of LNO to show remarkable results as SOFC cathode when exposed to a chromium source has been proven. Hou [10] studied the behavior of LNO as SOFC cathode in clean air and chromium-containing air for 20 hours while applying a current density of 200 $^{mA}/_{cm^2}$. The study showed the high tolerance of the material towards chromium by analyzing polarization resistances (R_p) and SEM pictures of the material and triple-phase area. It was concluded that chromium had little effect on the cathode's resistance polarization, therefore contributing to small polarization losses. The R_p of the cathode under exposure to chromium was roughly 0.6, which showed a small increment when compared to that of the same cathode at 0 hours. At the same time, this R_p was compared to that of an identical cathode that operated without a chromium source, which showed a slight difference in normalized values. Furthermore, SEM pictures showed visual proof of the electrochemical measurements. The pictures of both atmospheres before and after the operation were compared. The LNO cathode that operated under chromium-poisoned air did not show significant differences when compared to the picture of the LNO that operated under the absence of chromium sources. The structure of both materials was similar, as they both showed a uniformly porous structure. Furthermore, the cathode/electrolyte interface showed no chromium presence apart from the absence of voids and excellent adhesion of LNO on the GDC electrolyte, which translates into a more significant number and size of active sites where the electrochemical reaction between electrode and electrolyte is happening.

Longer studies on the behavior of LNO as SOFC cathode under chromium-containing air have been performed as well. Gong [9] studied the comparison of LNO and LSM under chromium sources operation when an external current is applied for six days. Results showed that the exposure to chromium of LNO did not only not cause an increase in resistance polarization but also decreased polarization losses and gave out an enhanced polarization resistance, both in dry and humidified air. On the other hand, LSM showed a significant increase in polarization resistance due to the same chromium exposure that LNO went through.

Another studied aspect of the influence of chromium on LNO is the effect that this external agent could have on phase stability or decomposition. Schrödl [26] focused on the phase decomposition of LNO after being exposed to chromium under dry and humid conditions. Samples ran at 800ºC for 600 hours under dry air without chromium exposure. Neither surface nor bulk seemed to have been damaged by operation since their diffusion coefficients did not show significant variations. Samples were then exposed to chromium from t = 600 to t = 1000 hours. The chemical surface diffusion coefficient (K_{chem}) was reduced by a factor of 1.3, which could reflect the chromium deposition on top of the electrode surface. On the other hand, the chemical diffusion coefficient (D_{chem}) did not show any significant impact; therefore, the bulk did not seem to have been affected. Results showed a noticeable change when the air was humidified. K_{chem} decreased by a factor of 18, with D_{chem} not being able to be extracted by means of the previously used methods, indicating a change in the location of the oxygen exchange reaction. When the atmosphere's humidity was increased (30% to 60% relative humidity) for another 1000 hours, K_{chem} suffered a slight decrease. Schrödl [26] concludes that this correlates with the small partial pressure increase of the most abundant chromium species $CrO_2(OH)_2$ (from 1.9 E-8 bar to 3.9 E-8 bar at 60% relative humidity). This study also compared the results of another of their studies. The influence of chromium and silicon (experiment performed in a quartz chamber) on the oxygen exchange kinetics of LNO was studied at 700ºC. After comparing, K_{chem} dropped by a factor of 230 at this temperature while showing an overall drop by a factor of 25 at 800ºC.

Although it has predominantly been regarded as a SOFC cathode, LNO's characteristics also make it a suitable candidate for SOEC anode material. A study by Flura [37] tested different composite materials with the formula $La_{2-x}Pr_xNiO_{4+\delta}$ at x = 0, 0.5, 1, and 1.5 in an R-SOC configuration. The theory behind the experiment was to determine at what point in composition the properties of both elements would reach an ideal proportion. Praseodymium was used due to its high electrochemical performance, while lanthanum was used due to its reliable stability. Regular RP phase LNO is found at x = 0 and was tested for thirty days under a current density of 300 $^{mA}/_{cm^2}$. Flura's results [37] showed that the electrochemical aging of LNO under SOEC conditions is stable (+180% after 1110 hours) while showing a fast degradation under SOFC conditions (1110% after 1100 hours). SEM pictures confirmed no significant degradation on the SOEC side while showing partial

delamination on the SOFC side, which could translate into an increase in both ohmic and polarization resistance. It is also concluded that the main difference between the performance of perovskite oxides such as LSM or LSCF and that of RP phase lanthanide nickelates is the ability to incorporate oxygen ions into the lattice, as stated before. Since the SOFC delaminated (probably due to external conditions), no conclusions could be drawn from it. On the other hand, the difference in SOEC mode performance accounts again for the ability of lanthanide nickelates to become hyper stoichiometric. A large inflow of oxygen ions from the electrolyte towards the electrode does not result in an overstocking of ions at the electrolyte/electrode interface, as they have sites within the electrode that they can occupy. The same process in perovskite-structure LSM and LSCF leads towards an over-concentration of oxygen at the perovskite electrode/electrolyte although the incapability of incorporating oxygen ions in the same way that LNO does can lead to a rapid delamination and operating failure.

While all these tests were mainly focused on the performance of LNO as SOFC Cathode, the results portrayed in this study show the performance of the material as both SOEC Anode and SOFC Cathode under chromium poisoning conditions for longer operational times, focusing on the prospective application of the material for R-SOCs. Different synthesis methods were applied for both testing and materials synthesis that could lead to differences in performance and long-term stability of the sample.

2. EXPERIMENTAL METHOD

The main goal of this experiment was to determine the long-term stability of Ruddlesden-Popper phase rare earth nickelates as oxygen electrodes for R-SOC in the presence of external chromium sources. Again, the presence of chromium replicates any external poisoning that metallic interconnectors could inflict in the electrochemical behavior of the cell as well as the physical appearance of the electrode when investigated.

2.1 CHARACTERIZATION

2.1.1 XRD Analysis

The major phase and structure of the cathode material was studied through X-ray diffraction (XRD, PANalytical X'pert PRO, $Cu\,Ka$ radiation). This testing can provide information about the purity of the compound as well as other secondary phases.

2.1.2 EIS Analysis

The electrochemical performance of the cell was measured through electrochemical impedance spectroscopy (EIS), carried out in a potentiostat station (Interface 1010, Gamry) that could carry this type of test. The selected frequency range that was used while testing was 1Mhz – 0.1 Hz. For the experiment, a 3-probe configuration was used, although there were two electrodes placed on the edges of the electrolyte. Only the third probe that was placed on the opposite side of the measured electrode was used while testing each electrode:

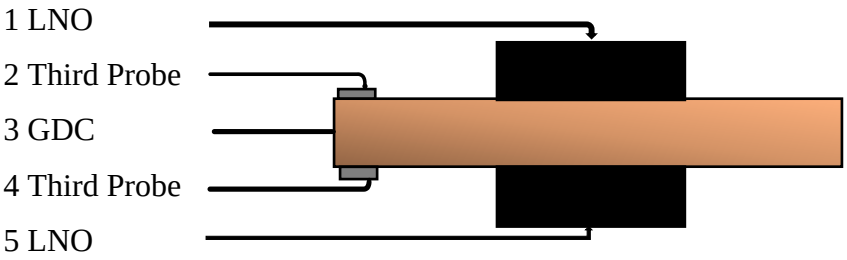

Figure 5: LNO/GDC symmetric cell

The potentiostat station provided a working probe, a reference probe, a working sense probe and a counter probe. This method allowed for a separation of the electrodes' resistances when taking measurements. Both electrodes started as equal at the beginning of the experiment but started changing their function by applying an external current that would flow from one electrode to the opposite. This allowed for an operational simulation in which the anode that received the current straight from the circuit became the SOEC Anode while the opposite started acting as a SOFC Cathode. By using the third-probe measurement, the resistance of both electrodes would be separated, therefore the reactions that were happening at the SOEC Anode did not affect the overall resistance of the SOFC Cathode and vice versa. The measurement starting point would be at the electrodes (1 and 5) and would stop at the third probe point (2 and 4). All EIS tests were performed under OCV conditions.

The electrochemical impedance spectroscopy (EIS) technique is used to characterize and analyze the behavior of electrochemical systems. Measurements in EIS are performed by applying a small perturbation to the system/cell in the form of either current or voltage sine waves. Once the perturbation has been applied, the measurement consists in collecting the response to the perturbation in the voltage or current, respectively. In this experiment, Nyquist plots will be the chosen graph to plot the results.

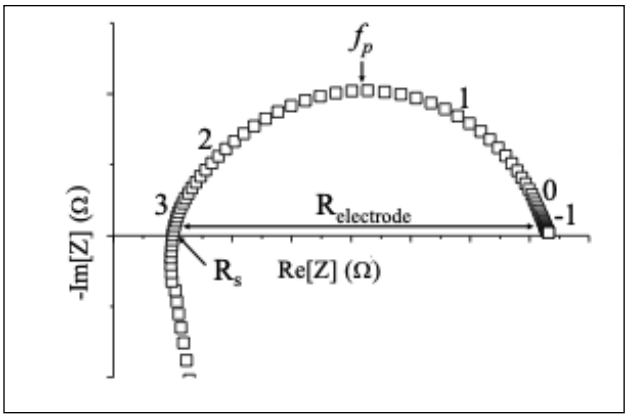

Figure 6: Example of Nyquist plot. The x-axis accounts for the real part of the impedance while the y-axis represents the imaginary part. R_s is ohmic resistance and $R_{electrode}$ represents polarization resistance [41].

.

As stated before, the EIS measurements were arranged in a 3-probe Set-up. The functionality of each electrode is explained in the table below:

Working	Designation for the electrode being studied. The point that stablishes where the measurement starts.
Working Sense	Responsible of applying the current that will go through the electrode.
Reference	Serves to establish the end point of the measurement. Isolates itself by having no current flowing through them.
Counter	End of current path.

Figure 7: Gamry probes roles

The working and the working sense probes were tied together at point W/WS while the reference probe was attached at R. Counter electrode is represented at C. This way, the cell was only measured from W/WS to R. The corresponding resistance of the counter-side reaction did not inflict in the measured resistance.

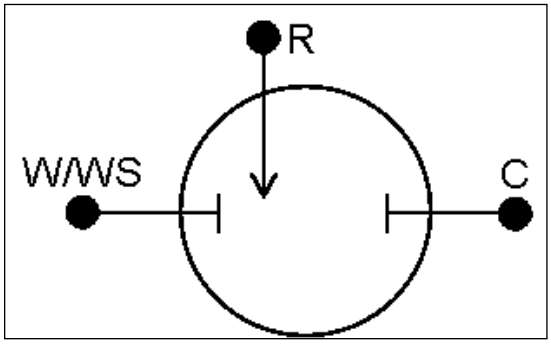

Figure 8: 3-probe electrode set-up [41]

2.1.3 SEM Observation

SEM pictures (JSM 7600F Scanning Electron Microscope, JEOL) of the cross-section of the samples were taken to observe the microstructure of the electrodes as well as to determine whether the densification of the electrolyte pellet was enough to conduct the experiment. Interface was also taken into consideration, as poor bonding would result in deficient electrochemical results. Before using SEM, pellets were sputtered over with a gold/palladium mixture in a sputter and carbon coater (Desk V Sputter and Carbon Coater, Denton) covering the whole cross-section of the cell. This allowed electrons to move all over the surface. Otherwise, electrons might have stayed constrained in one area and the produced noise would not have allowed for the sample to be investigated. EDX spectroscopy was performed on the samples after being exposed to external chromium sources.

2.1.4 Distribution of Relaxation Times Deconvolution

Distribution of relaxation time (DRTTools, MATLAB) was used in order to express the electrochemical performance of the cell as a function of time instead of frequency. This allows the user to identify the different steps in the reaction that would not be able to be distinguished from each other in an EIS plot. The attributed resistance of each step is also separated and expressed in the plot, observing how the cell performs in each of the steps of the process.

2.2 CELL FABRICATION

2.2.1 LNO Synthesis

$La_2NiO_{4+\delta}$ was the chosen material to perform as oxygen electrodes (SOEC Anode and SOFC Cathode) due to a higher stability than praseodymium nickelate (PNO, $Pr_2NiO_{4+\delta}$) and a better electrochemical performance than neodymium nickelate (NNO, $Nd_2NiO_{4+\delta}$). The final product was achieved through sol-gel method achieving a 1:1.25:1.25 ratio (Nitrates: Citric Acid: EDTA). Nickel and lanthanum nitrates were arranged and measured in a stoichiometric ratio to obtain the desired RP phase. Reactants were dissolved

in deionized water and citric acid was added to the mixture. Once a homogeneous mixture was achieved, ethylenediaminetetraacetic acid (EDTA) was added to the solution as a complexing agent along with ammonia to control the mixture's pH and adjust it to 8. Once all reactants were combined, the mixture was heated up to 280ºC until gelation occurred. The mixture was left at 200ºC overnight until drying up and was left at 500ºC for 24 hours to ensure all organics in the mixture were burnt out. The last step of the process involved sintering powder at 1100ºC for 4 hours. The final product was taken through x-ray diffraction (XRD, PANalytical X'pert PRO, Cu Ka radiation) measurements.

2.2.2 GDC Electrode synthesis

This study was performed using electrolyte supported cells (also known as half-cells or symmetrical cells). For the electrolyte material, gadolinium-doped ceria (GDC 20%, Fuel Cell Materials) was chosen due to its high compatibility with LNO, as previously mentioned. GDC powders were ground after being dissolved into a 3% polyvinyl butyral (PVB, Aldrich) – ethanol solution. Once a homogeneous solution was achieved, it was ground until all ethanol evaporated, leaving only binder and GDC behind. Once the components were ground together into a fine powder, they were taken into the press, where they were pressed into 20 mm radii pellets after applying a 15000 lbs. force on them. They were then sintered at 1500ºC for 5 hours. The experimental procedure does not match with previously reported sintering temperatures, as there still is some discrepancy over the ideal sintering temperature of GDC. Pellets were initially sintered at 1400ºC and 1450ºC, although they did not offer a good bonding when LNO electrodes were applied, resulting in poor electrochemical performance. Only when the sintering temperature was raised up to 1500ºC and sintering time was extended from 4 to 5 hours, the electrochemical behavior of the cell matched similar reported results in ohmic resistance as well as in polarization resistance.

2.2.3 Assembling of the cell

An LNO slurry was prepared by adding ink vehicle (VEH, Fuel Cell Materials) to the LNO powders that were obtained after sintering. The mixture was ground in a mortar until a homogeneous slurry was obtained. This slurry was then applied on both sides of the GDC

pellets by hand-brushing and dried up at a temperature between 150ºC-175ºC only for the purpose of drying up the slurry and to make the handling of the pellets easier. Once dry, symmetrical cells were sintered at 1150ºC for 2 hours, using a ramping of 3ºC/minute. More explanation of the chosen temperature for LNO sintering will be given in the Results and Discussion section. Silver paste was applied on the surface of both electrodes as well as a small dot on the edge of both sides of the electrolyte so a 3-electrode measurement could be performed.

2.2.4 Chromium Source Synthesis

To simulate the effect that a metallic interconnector would have on the cell, the cell had to be exposed to an external porous chromium source (this would help with chromium evaporation and transport). Cr_2O_3 was the chosen material for this role, as it would simulate the possible delamination of the chromia scale at the surface of the MIC. Cr_2O_3 powders were weighed and mixed with starch and PVB in a ratio of 100:10:3 (chromium oxide: starch: PVB) in weight. Powders were then dissolved in ethanol and ground until all ethanol evaporated. The homogeneous mixture of powders was then taken into pellet pressing, using a 6mm-radii dye. Once pellets had been pressed, they were heated up to 350ºC for 1 hour to get rid of both PVB and starch. The chosen ramping for this process was 2ºC/min, as pellets might not have resisted a faster ramping since their mechanical strength was low at this point. Samples were naturally cooled down to room temperature and sintered at 1100ºC, staying isothermal for 6 hours.

The first approach towards the fabrication of MIC replication chromium source consisted of a chromium-impregnated alumina wool but was not successful. The reason could be the characteristics of the aluminum, since Al-containing-alloys are sometimes used as a protective/preventive layer for chromium evaporation in BoP. Another reason could have been the uneven airflow that would come out of the wool, since an even placement inside the 1-inch bore was not accurate. Therefore, the synthesis of porous chromium pellets seems like a more suitable choice to produce and measure accurate results.

2.3 TESTING SET-UP

Two tubular furnaces containing a dual chamber were used to perform P_{o2} measurements as well as long-term stability testing. Each of these chambers consisted of a 1-inch radii hollow alumina tube (AdValue Technology) which was able to accommodate one single holder per chamber. These holders were put through a bored rubber stopper (chamber sealant) and consisted of a 4-bore alumina tube through which silver wires were running and attached to the current collector silver paste applied on the electrode. A U-shaped platform was attached to the end of the tube using Ceramabond (Aremco) on which the cell would rest in a horizontal position, allowing the airflow to reach both electrodes equally and allowing it to promote one reaction as much as the other. Regular air (P_{o2} = 21%) was flown into the chamber through the other side of the tubular chamber at a rate of 200 sccm. Once both sides of the chamber were sealed with stoppers, the cell was heated up to 700ºC and held isothermal for 500 hours. Two different environments were tested to compare results at t = 500 hours. One of them was run under clean air conditions while the second one was tested under chromium poisoned air. The operation was run under galvanostatic conditions in which the total DC current applied was 900 mA. Considering that the area of the electrode was 0.3167 cm^2, it can be concluded that cells were running at a current density of 0.03 $A/_{cm^2}$, simulating common operating conditions.

3. RESULTS

3.1- XRD

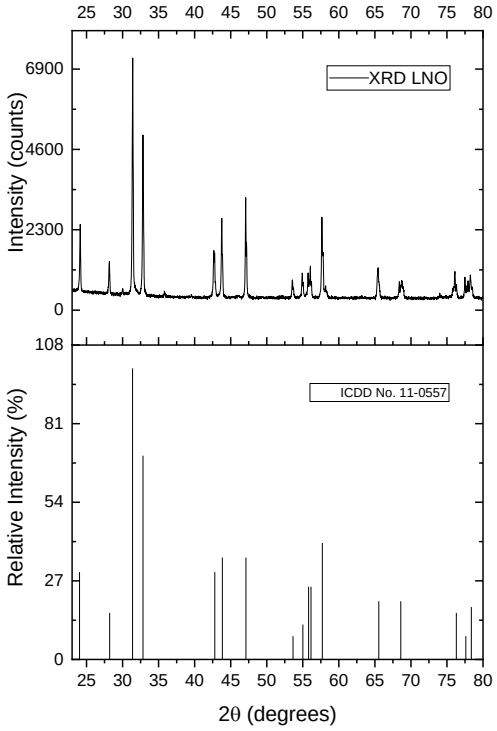

Figure 9: X-Ray Diffractometry of LNO. Reference PDF #11-0557.

The previous figure is the plot of the RP-Phase LNO that was used throughout the whole experiment. The analysis confirmed the achievement of the desired structure in which perovskite $LaNiO_3$ layers will alternate with LaO layers along the lattice's c-axis. When comparing the plot with an external reference LNO, a major RP-Phase LNO with a small La_2O_3 impurity at 30º was revealed. This impurity is not expected to affect results in any way since it is not expected to react with any other material in the major $La_2NiO_{4+\delta}$ phase. Therefore, the XRD confirmed that the results are reliable from a phase-stability point of view.

3.2 LNO SINTERED AT DIFFERENT TEMPERATURES

Different temperatures were used to sinter LNO ranging from 100ºC to 1200ºC in order to choose the temperature that would give better results both in performance and stability. EIS graphs of sintering temperatures of 1000ºC, 1100ºC, and 1150ºC were collected. LNO sintered at 1200ºC was not put through EIS, although it was observed under SEM. The structure of the material seemed not porous enough, which would make it more complicated for the gas diffusion process to happen, and for the oxygen ions to hop through until reaching the electrolyte once the oxygen molecule had been dissociated. The following figures correspond to the Nyquist plot of the performed EIS on an LNO symmetrical cell and the SEM picture of the LNO-GDC interface respectively. The EIS analysis that was performed on the samples that were sintered at different temperatures was analyzed through a regular two-probe configuration. No polarization was applied in order to confirm the best performance among them before using them in long-term testing.

3.2.1-LNO sintered at 1000ºC.

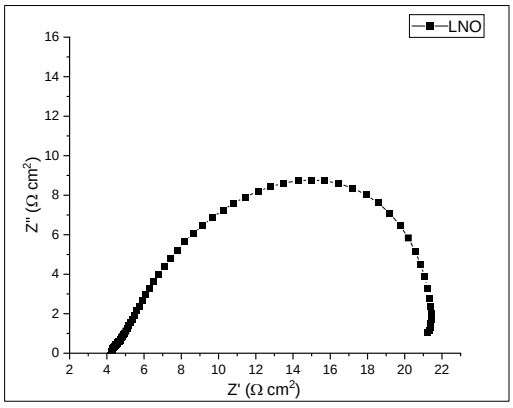

Figure 10: Nyquist plot of LNO electrode sintered at 1000 ºC. Testing performed at 700 ºC.

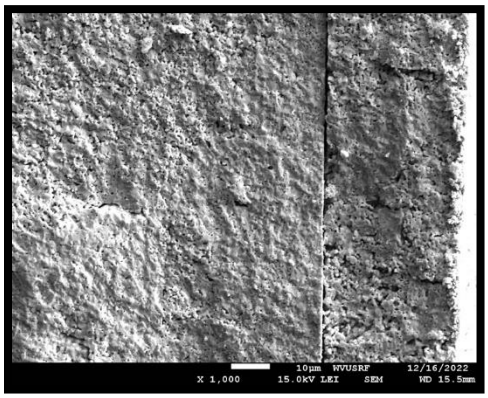

Figure 11: SEM picture of the LNO-GDC interface. Testing perfrormed at 700 ºC

Two main outputs were taken out of the EIS analysis of the sample sintered at 1000ºC. First is a large ohmic resistance, corresponding to the GDC electrolyte, located at $R_s \cong 4\ \Omega cm^2$. This value is too big for a GDC electrolyte. Then a larger polarization resistance, corresponding to the electrodes of the cell, at $R_p \cong 17\ \Omega cm^2$. These results showed a deficient performance of the cell, as the targeted resistance was much lower.

These values pointed towards a: possible delamination of the cell, although unlikely, as the sample had been exposed to a slow ramping (3ºC/min) which should not have induced a big mechanical stress in the cell due to the thermal expansion of the components; or a poor bonding of the components at the electrode/electrolyte interface. SEM pictures confirmed a minimal bonding between the electrode and electrolyte with almost no contact between layers. This ends in big losses, both ohmic and polarization related. As stated in previous sections, the larger the area of the reaction, the better the reaction is going to be. Samples were repeated to check a behavioral pattern, achieving similar results. Sample observation under SEM checked the second theory.

3.2.2- LNO sintered at 1100ºC.

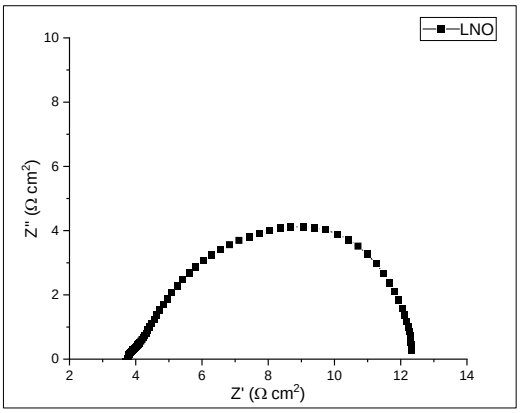

Figure 12: Nyquist plot of LNO electrode sintered at 1100 ºC. Testing performed at 700 ºC.

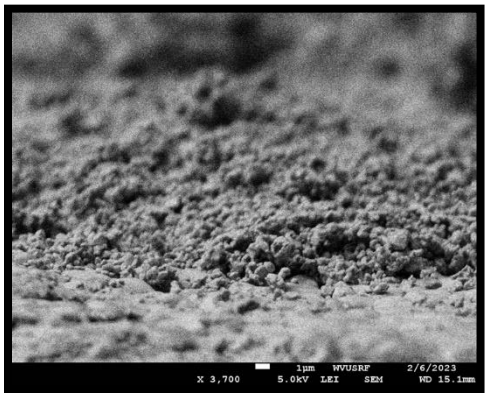

Figure 13: SEM picture of the LNO/GDC interface. LNO was sintered at 1100 ºC.

EIS analysis of the sample showed almost no decrease in R_s but showed a $R_p \cong 8\ \Omega cm^2$. That is roughly a 9 Ωcm^2 difference with respect to the LNO sintered at 1000ºC. That shows an improvement in bonding at the electrolyte/electrode interface, although R_p is still too large to put samples through stability testing. LNO shows a better bonding to the electrolyte surface but shows almost no cohesion between particles. It must be stated that the breaking of the sample to analyze the cross-section must have peeled off most of the surface layer, leaving a thin bulk layer on. On the other hand, most of the bulk and surface layer should have stayed on the electrolyte's surface if proper bonding had been achieved. Lack of cohesion between grains made it harder to capture clearer pictures of the interface.

3.2.3- LNO sintered at 1200ºC.

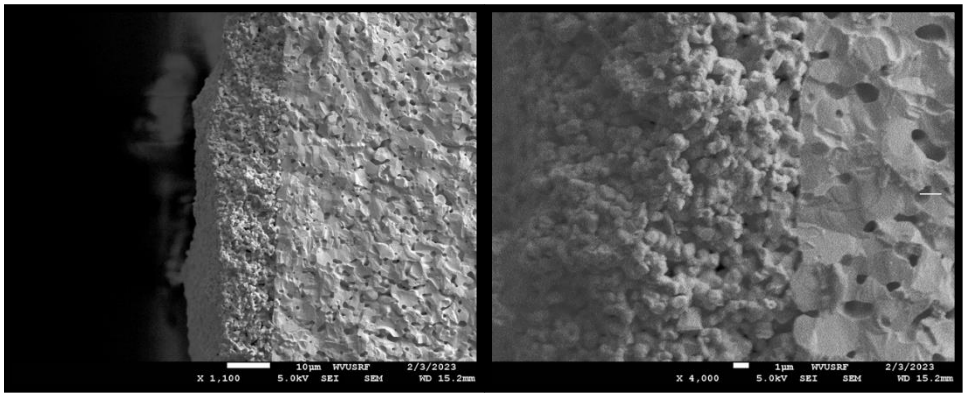

Figure 14: SEM pictures of the LNO/GDC interface. LNO was sintered at 1200 ºC

SEM observation was the only analysis that was performed on LNO sintered at 1200ºC. When observing under increased magnitude, good bonding between layers was observed, increasing the number of active regions on the electrode/electrolyte interface. The porous structure of the LNO was deemed not porous enough for the ORR/OER to perform efficiently. Since the number and size of the pores in the layer decreased, oxygen ions would not have enough pathways to go through the electrode and reach the electrolyte.

3.2.4- LNO sintered at 1150ºC.

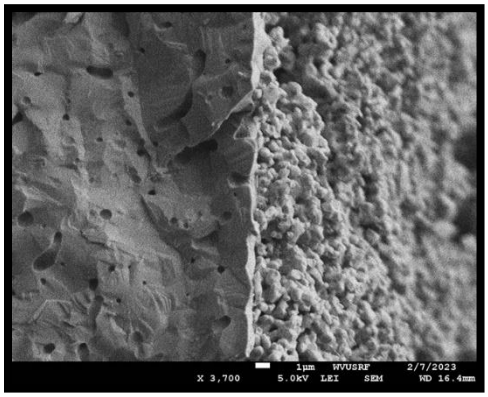

Figure 15: SEM pictures of the LNO/GDC interface. LNO was sintered at 1150 ºC.

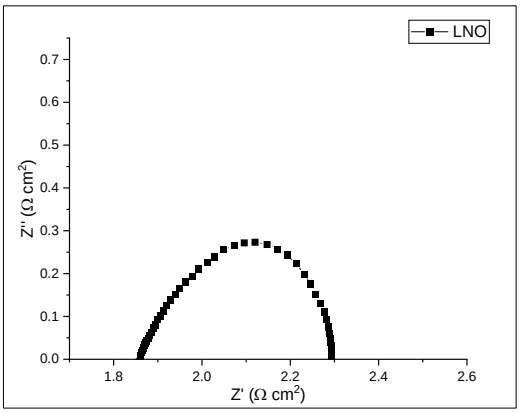

Figure 16: Nyquist plot of LNO electrode sintered at 1150 ºC. Testing performed at 700ºC.

LNO sintered at 1150ºC showed a much better performance than that of its predecessors. R_s decreased down to $R_s \cong 1.8\ \Omega cm^2$, decreasing by almost 2.5 Ωcm^2 compared to that of LNO sintered at 1100ºC and 1150ºC. R_p went down to $R_p \cong 0.4\ \Omega cm^2$. This decrease in both ohmic and polarization losses leads towards a proper bonding at the electrode/electrolyte interface, as well as a great cohesion between LNO grains. These results concluded that 1150ºC is a more adequate sintering temperature for RP-phase LNO than lower temperatures. Again, results on LNO sintered at 1200ºC were not performed due to the observations in grain cohesion as well as bonding at the interface. The behavior of a sample with those characteristics was yet to be known at the moment of the experiment.

3.3- LONG STABILITY TESTING UNDER REGULAR AIR CONDITIONS

The main section of the experiment consisted in the long-term stability testing of the electrochemical performance of RP-phase LNO as oxygen electrode for R-SOCs under chromium exposure for 500 hours. For that, samples had to be tested in the same conditions without external chromium sources.

3.3.1- SOEC Anode mode

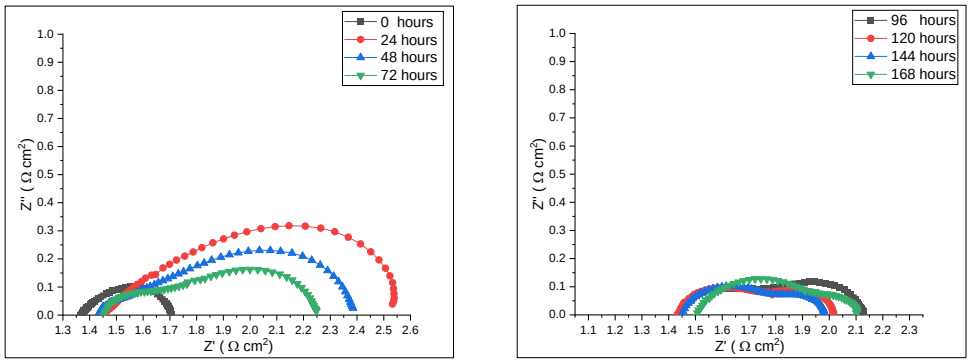

(a) (b)

Figure 17: Nyquist plots of LNO performing as SOEC anode from (a) 0 to 72 (day 3) hours and (b) 96 (day 4) to 168 (day 7) hours.

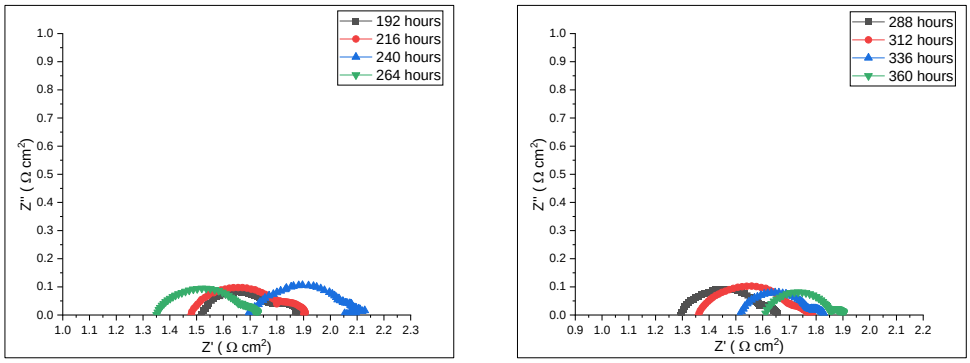

(a) (b)

Figure 18: EIS plots of LNO performing as SOEC anode from (a) 192 (day 8) to 264 (day 11) hours and (b) 288 (day 12) to 360 (day 15) hours.

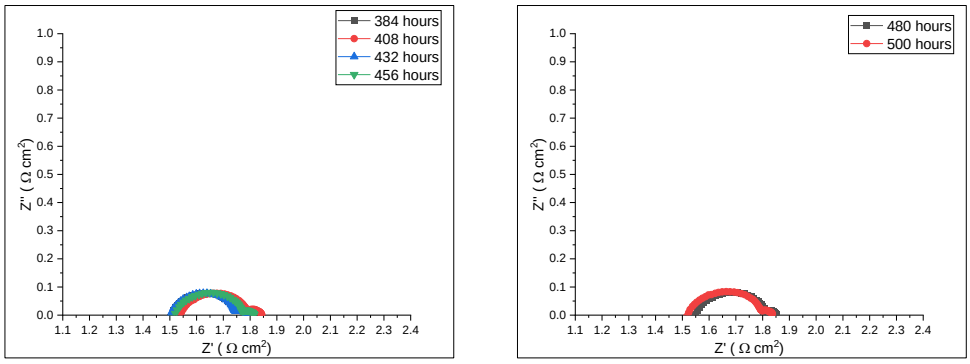

(a) (b)

Figure 19: EIS plots of LNO performing as SOEC anode from (a) 384 (day 16) hours to 456 (day 19) hours and (b) 480 (day 20) to 500 (day 21) hours.

As can be seen, the polarization resistance of the electrode tended towards stabilization with the passing of time. Multiple samples show similar behavior after the first 24 hours under polarization, showing a peak in R_p with a consequent progressive decrease until stabilization throughout the second half of testing. The sample showed a R_p peak at $R_p \cong 1.1\ \Omega cm^2$ after 24 hours and finished the experiment at $R_p \cong 0.3\ \Omega cm^2$. Initial $R_p \cong 0.35\ \Omega cm^2$ Results will be discussed and analyzed in the conclusion section.

3.3.2- SOFC Cathode Mode

Same tests were performed on the other electrode, which was performing as SOFC cathode due to the current flow. The following figures correspond to the performance of the electrode as SOFC cathode under clean air conditions.

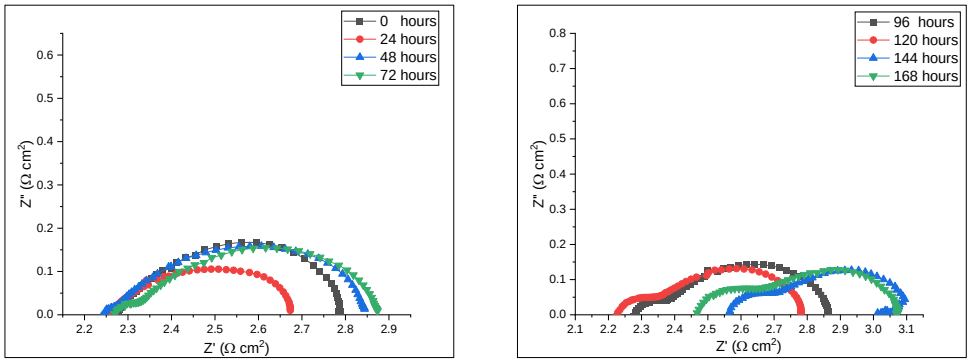

(a) (b)

Figure 20: EIS plots of LNO performing as SOFC cathode from (a) 0 to 72 hours (day 3) and (b) 96 (day 4) to 168 (day 7) hours.

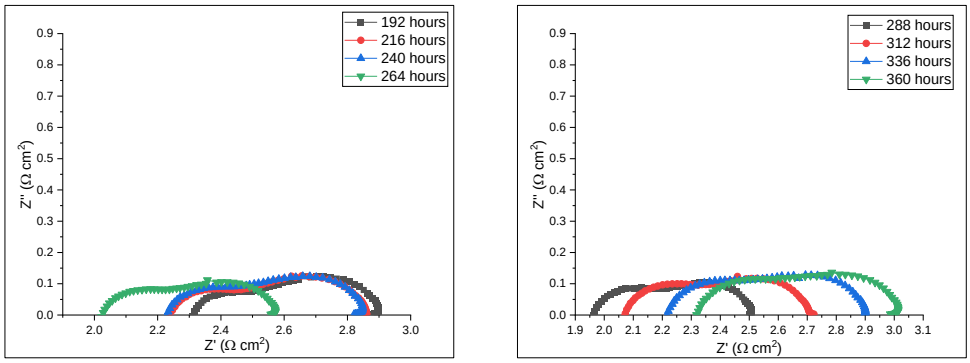

(a) (b)

Figure 21: EIS plots of LNO performing as SOFC cathode from (a) 192 (day 8) to 264 (day 11) hours and (b) 288 (day 12) to 336 (day 15) hours.

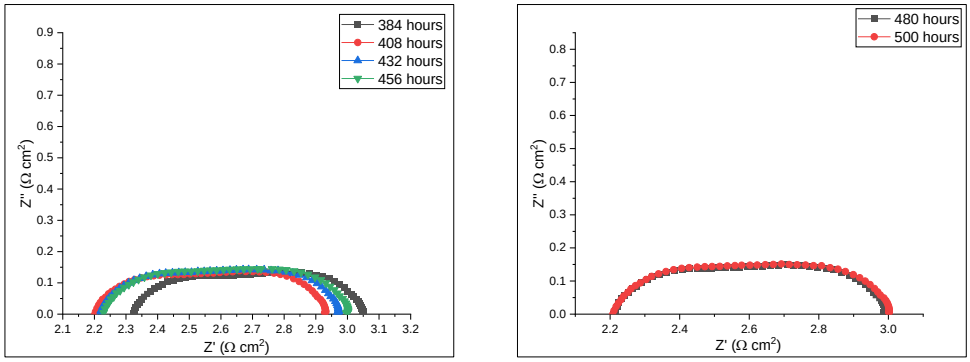

(a) (b)

Figure 22: EIS plots of LNO performing as SOFC cathode from (a) 384 (day 16) to 456 (day 19) hours and (b) 480 (day 20) to 500 (day 21) hours

Same as its counterpart, the electrode running in SOFC cathode mode showed a progressive stabilization throughout the second half of testing. On the other hand, the cathode showed a small decrease throughout the first 24 hours under polarization, opposite to the anode. Initial $R_p \cong 0.5\ \Omega cm^2$ and went down to $R_p \cong 0.4\ \Omega cm^2$ after the first day. Final $R_p \cong 0.85\ \Omega cm^2$. Results will be discussed in the conclusion section.

3.4- LONG TERM STABILITY TESTING UNDER CHROMIUM CONDITIONS

The following subsection consists of the analysis of the samples that were exposed to Cr_2O_3 pellets for 500 hours. Data was collected every 24 hours and analysis was performed

under OCV conditions. Chromium oxide samples weighed an estimated of 2g before operation. The following figures correspond to the Nyquist plots of both electrodes of said samples:

3.4.1- SOEC Anode

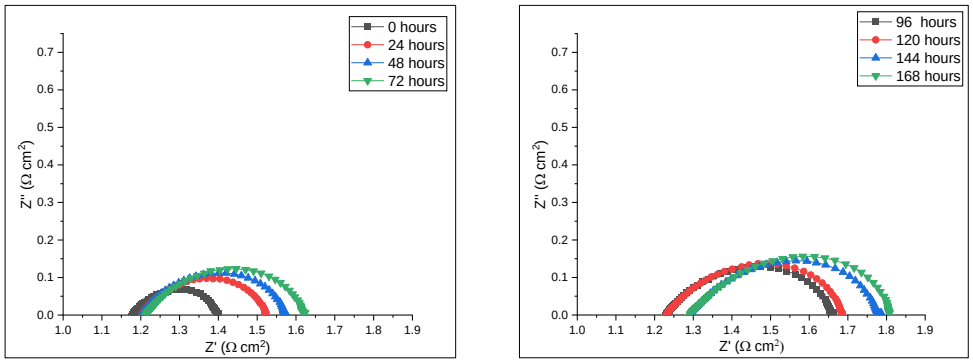

(a) (b)

Figure 23: Nyquist plots of LNO in SOEC anode mode from (a) 0 to 72 (day 3) hours) and (b) 96 (day 4) to 168 (day 7) hours.

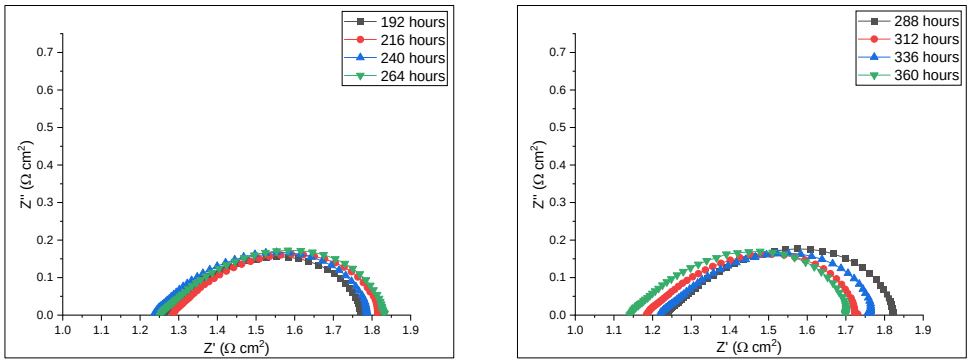

(a) (b)

Figure 24: Nyquist plots of LNO in SOEC anode mode from (a) 192 (day 8) to 264 (day 11) hours and (b) 288 (day 12) to 360 (day 15) hours.

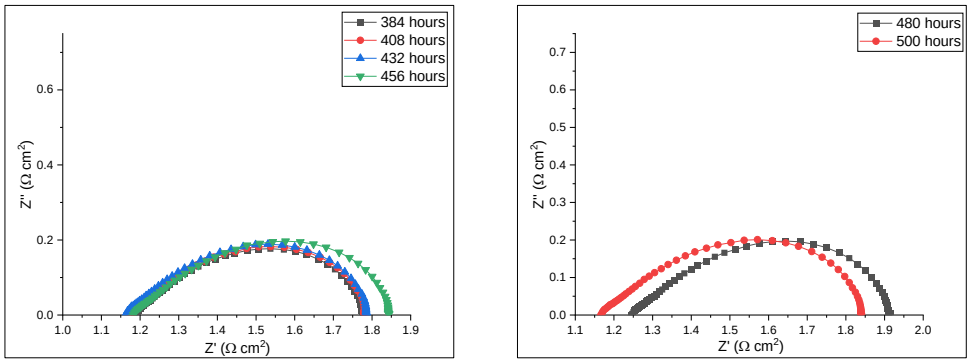

(a) (b)

Figure 25: Nyquist plots of LNO in SOEC anode mode from (a) 384 (day 16) to 456 (day 19) hours and (b) 480 (day 20) to 500 (day 21) hours.

The SOEC anode electrode showed a more progressive degradation throughout the 500 hours and a relative stabilization in R_p around day 12. The peak in R_p was seen in day 15 in which $R_p \cong 0.7\ \Omega cm^2$ although the stabilization was seen at $R_p \cong 0.6\ \Omega cm^2$.

3.4.2- SOFC Cathode

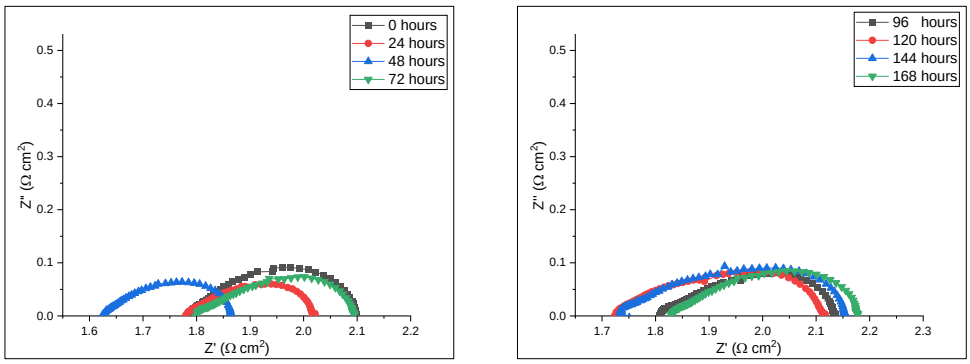

(a) (b)

Figure 26: Nyquist plots of LNO in SOEC anode mode from (a) 0 to 72 (day 3) hours and (b) 96 (day 4) to 168 (day 7) hours.

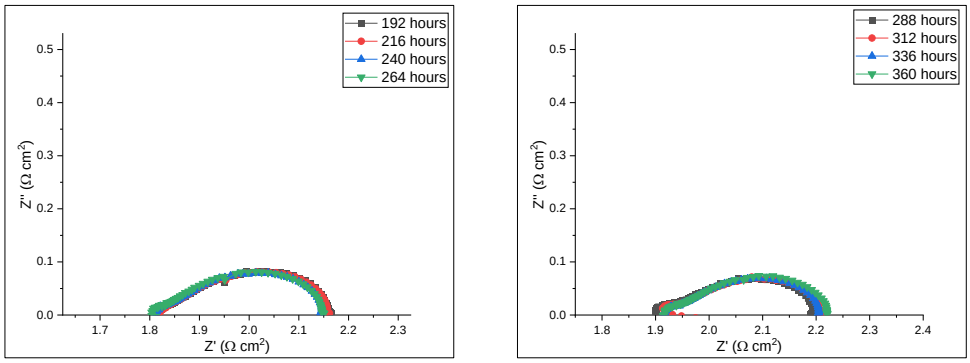

(a) (b)

Figure 27: Nyquist plots of LNO in SOEC anode mode from (a) 192 (day 8) to 264 (day 11) hours and (b) 288 (day 12) to 360 (day 15) hours.

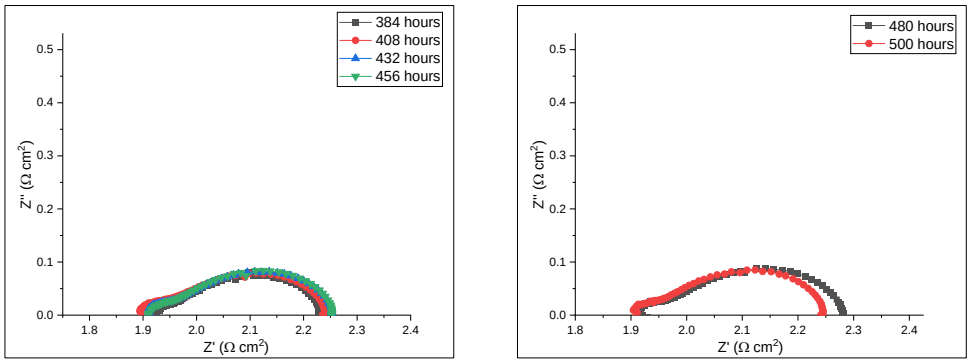

(a) (b)

Figure 28: Nyquist plots of LNO in SOEC anode mode from (a) 384 (day 16) to 456 (day 19) hours and (b) 480 (day 20) to 500 (day 21) hours.

Results showed that although the initial $R_p \cong 0.3\ \Omega cm^2$, the electrode showed no signs of degradation when looking at the electrochemical performance throughout the 500 hours. The peak $R_p \cong 0.4\ \Omega cm^2$ is seen after 8 days under polarization and chromium exposure.

3.4.3- Development of Polarization Resistances

In order to get a better sense of how Polarization Resistance values developed throughout the 500 hours, a comparison between both sides under chromium exposure was plotted against that of identical samples running under clean air conditions.

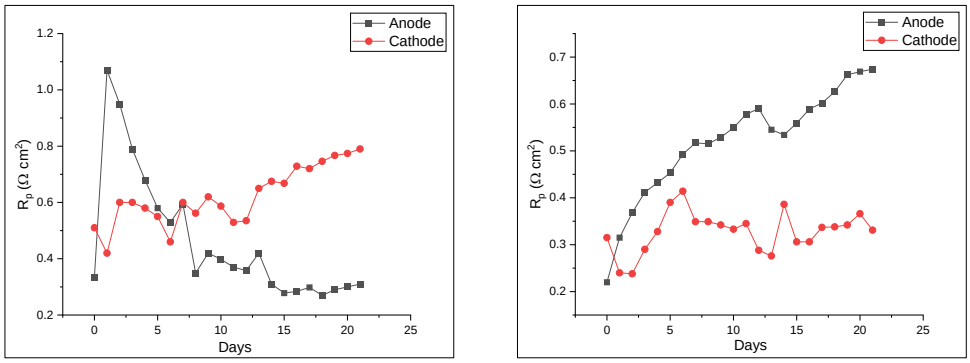

(a) (b)

Figure 29: Polarization Resistance under (a) clean-air conditions and (b) chromium exposure.

3.5 SEM OBSERVATIONS

3.5.1 SEM figures of SOEC Anode under clean-air conditions

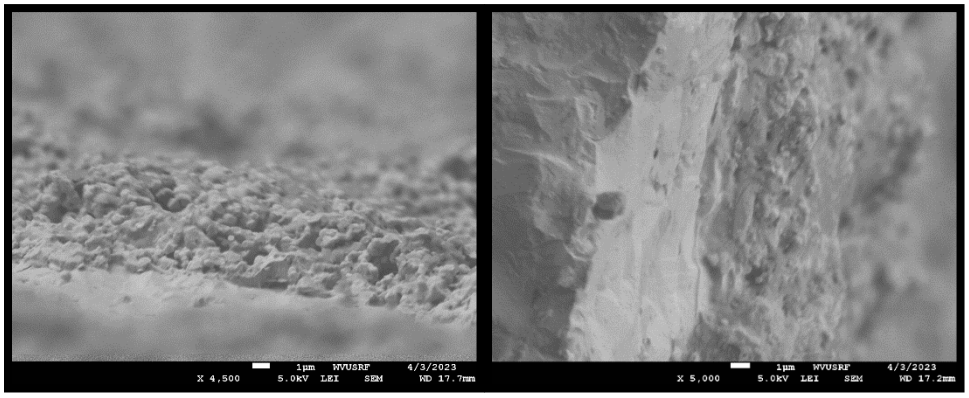

(a) (b)

Figure 30: SEM Figures of SOEC Anode exposed to clean air conditions for 500 hours at different magnitudes (a) and (b). In picture (a) the GDC layer is seen on the bottom part of the image while GDC is located on the left side of picture (b)

3.5.2 SEM figures of SOFC Cathode under clean-air conditions

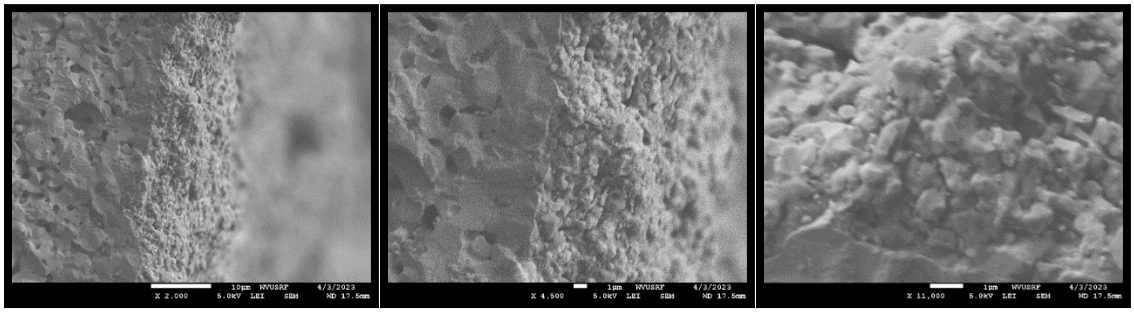

Figure 31: EM Figures of SOFC Cathode exposed to clean air conditions for 500 hours at different magnitudes. In pictures (a) and (b), the GDC electrolyte is located on the left of the image.

3.5.3 SEM Figures of SOEC Anode under chromium exposure

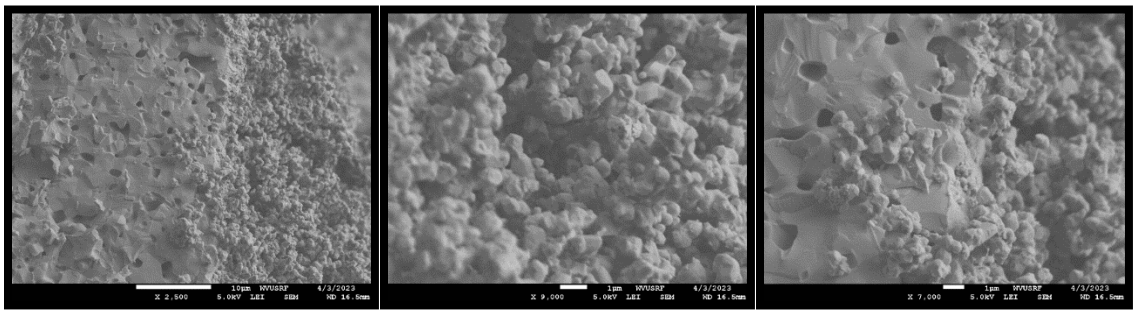

Figure 32: SEM Figures of SOEC Anode exposed to chromium conditions for 500 hours at different magnitudes. Figure (a) focuses on the GDC-LNO interface. Figure (b) zooms in to focus on the LNO electrode in order to get a better image of the grains. Figure (c) shows an increased zoom on the LNO-GDC interface

3.5.4 SEM Figures of SOFC Cathode under Chromium exposure

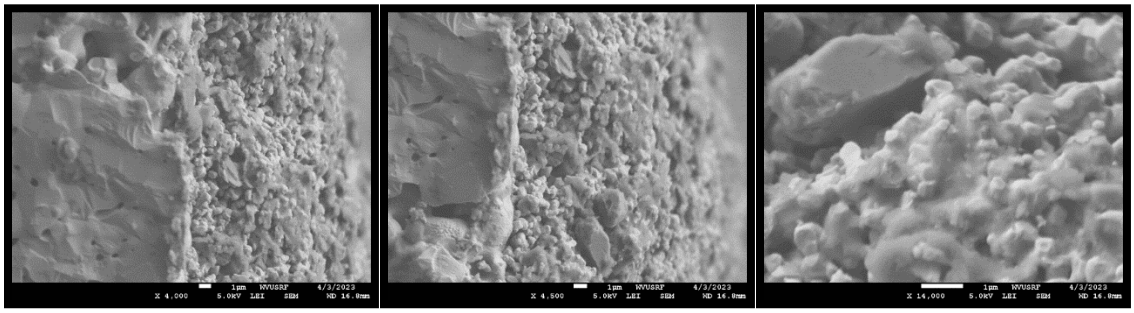

Figure 33: SEM Figures of SOFC Cathode under chromium exposure for 500 hours at different magnitudes. Pictures (a) and (b) focus on the GDC-LNO interface at different but similar magnitudes. Picture (c) focuses on the LNO grain size.

3.5.5 EDX Spectroscopy

In order to make sure that chromium had reached both the SOEC Anode and SOFC Cathode, an EDX spectroscopy was performed on both sides of the pellet. A scanning test was performed on both electrodes which confirmed the presence of chromium on both the SOEC Anode and SOFC Cathode. As seen in the plots, the La Lβ2 peak located at ≈ 5.1 KeV and the peak that corresponds to Cr Kα at ≈ 5.3 KeV can overlap. This interfered in the quantification of chromium on both electrodes although it is assumed that the even airflow distribution in the chamber reached both sides of the pellet equally.

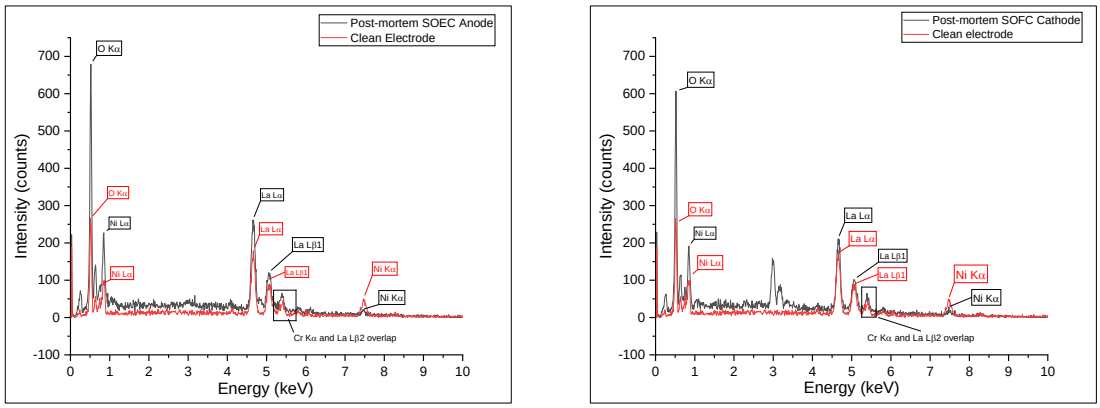

(a) (b)

Figure 34: EDX Spectroscopy of (a) SOEC Anode and (b) SOFC Cathode after long-term testing under chromium exposure. Red plot represents the electrode before operation.

3.6 DRT DECONVOLUTION

This section contains the deconvolution of the Distribution of Relaxation Times of the EIS Nyquist plots that were collected. Modifying the external conditions in the experiment such as temperature, oxygen partial pressure, chromium presence or polarization can induce changes in the behavior of the sample that is being tested. These modifications can affect every mechanism within the electrochemical reaction or, on the contrary, affect a specific step in the reaction.

The following DRT plots correspond to some of the EIS data that gave a better insight into how these processes were taking place inside the cell as well as how much each of them

was contributing to the cell's overall polarization resistance. The data that was collected on the first and last day of the samples that were running under both clean-air and chromium-poisoning conditions were analyzed and deconvoluted to identify which steps were being damaged by the chromium exposure. The oxygen partial pressure was increased after the long-term testing to see which step would be most influenced by the presence of oxygen in the environment. These two external conditions proved to be the most helpful ones for assigning an electrochemical mechanism to some of the peaks that are portrayed in the following plots.

3.6.1 SOEC Anode

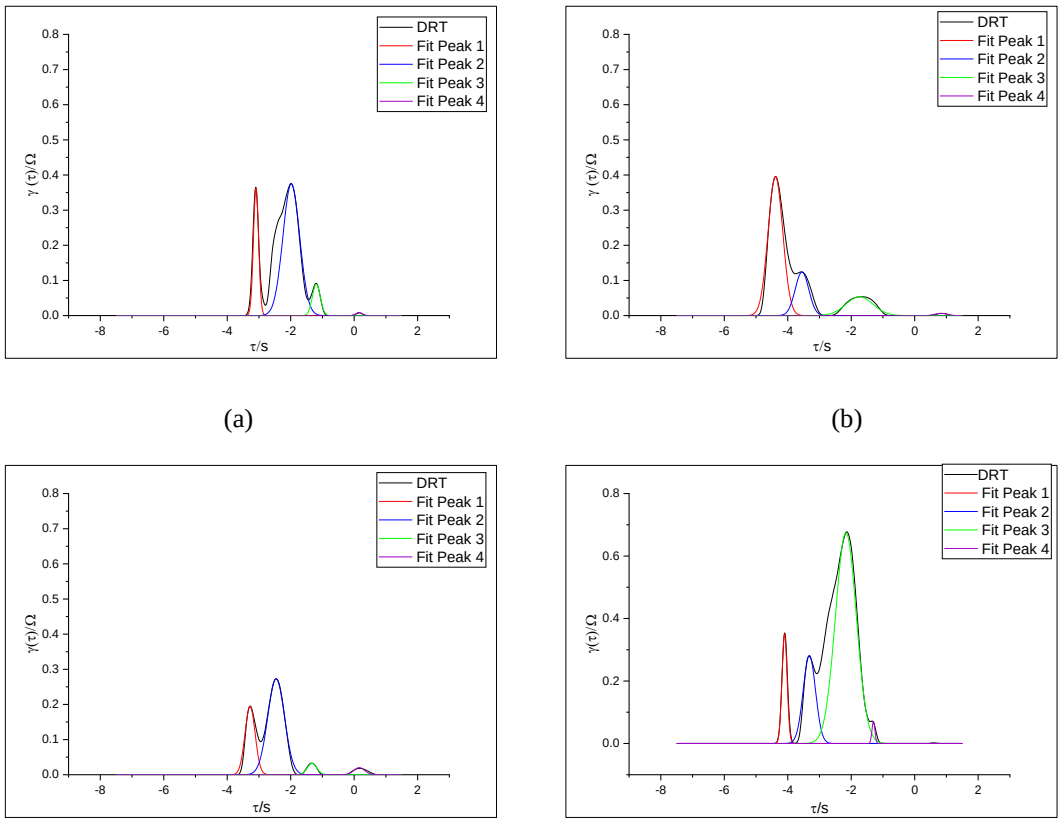

Figure 35: (a) and (b) show the DRT deconvolution of the SOEC Anode side at 0 and 21 days respectively. (c) and (d) correspond to the SOEC Anode side performing under chromium exposure at 0 and 21 days.

3.6.3 SOFC Cathode

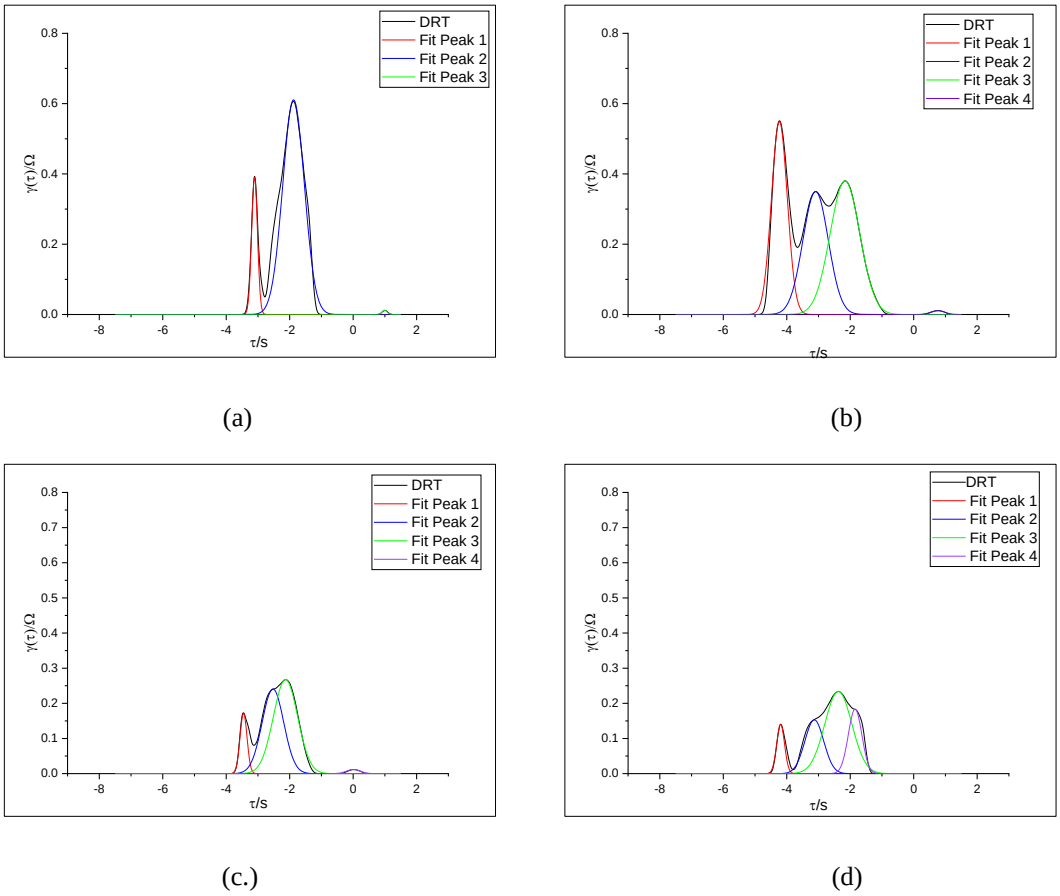

Figure 36: (a) and (b) show the DRT deconvolution of the SOFC Cathode side at 0 and 21 days respectively. (c) and (d) correspond to the SOFC Cathode side performing under chromium exposure at 0 and 21 days

3.6.4 DRT deconvolution under different Po2 levels.

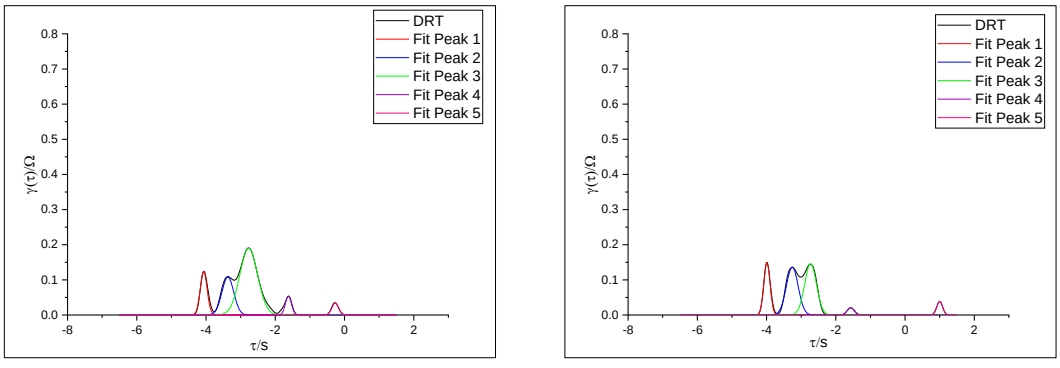

Figure 37: DRT deconvolution of the LNO electrode at 0 hours under (a) regular air and (b) 40% P_{O2}

As stated before, the previous plots showed the DRT deconvolution at specific times during the experiment. A Gaussian distribution was used in order to deconvolute and fit the peaks (blue, red, green, purple, and pink lines) underneath the shape of the original collected data (black line). Although the software showed the processes underneath the original shape, the fitting had to be manually adjusted in order to achieve higher accuracy when finding the fraction of the resistance that belonged to each individual process. The main differences between plots as well as the behavior of the different peaks under different conditions will be analyzed in the conclusion section in order to get a better insight into the electrochemical performance results of the LNO electrodes.

4. RESULTS ANALYSIS

In this section, the previous results will be analyzed in order to assess a proper understanding of the electrochemical behavior and performance of the LNO electrodes under chromium exposure throughout the experiment. It must be stated that none of the chromium species that could have been formed during the experiment were characterized or studied since they have already been reported in previous studies.

Before getting into the results of the experiment, the proper functioning of the cell was checked. It was determined that the cell's performance was valid to operate under long-term testing due to the initial performance of multiple samples at 0 hours. The reversibility of the cell was also proven by reversing the way of the current, therefore turning the SOEC Anode into SOFC Cathode and vice versa. Once these aspects were detailed, the characterization of the samples was collected and will be discussed in the following sub-sections.

4.1- EIS ANALYSIS UNDER CLEAN AIR

The first aspect of the experiment that must be addressed is the EIS data that was collected after 21 24-hour cycles under clean air. The initial performance of both SOEC Anode and SOFC Cathode were deemed as good results at $R_p \cong 0.35, 0.5\ \Omega cm^2$ respectively. The difference in initial performance was not understood as an indicator of prospective difference in electrochemical stability of each side in the long run, as such a small difference could be attributed to external factors such as a small difference in the airflow distribution and exposition from each side.

After 24 hours, both sides showed a different response to polarization. The R_p of the SOEC Anode increased up to 1.08 Ωcm^2, while the SOFC Cathode showed a small decrease down to 0.43 Ωcm^2, which could almost have been negligible if it had not been because this decrease was also seen in previously tested samples, establishing a pattern that must be addressed. This decrease in SOFC Cathode R_p followed by a small increase that leads to stabilization has previously been reported by Gong [9]. It is reported that this decrease in R_p could be caused by an improved bonding at the GDC/LNO interface that would be checked when analyzing the post-mortem microstructure of the sample. On the other hand, the

increase in R_p in the SOEC Anode after 24 hours leads to a progressive decrease in R_p until stabilizing at $R_P \cong 0.3\ \Omega cm^2$, which is like the one that the sample showed at 0 hours. This effect of polarization has also been previously reported by Jae Kim, although no explanation was found or given in the report. These phenomena still need deeper studying and understanding.

Overall, the performance of the sample was stable throughout the experiment. SOEC Anode found a relative stabilization around 216 hours while the SOFC Cathode needed around 312 hours to reach that stabilization. At the end of the experiment, the SOEC Anode showed a lower degradation rate than that of the SOFC Cathode

4.2- EIS ANALYSIS UNDER CHROMIUM EXPOSURE

The performance of the LNO electrodes under chromium exposure showed lower degradation rates in the long run than expected. The initial R_P of the SOEC Anode and SOFC Cathode were $R_P \cong 0.2, 0.3\ \Omega cm^2$ respectively. Again, that initial difference did not show any impact on the future degradation rate of the electrodes. The effect of chromium could be seen in the first 24 hours of operation.

On the side of the SOEC Anode, the increase in R_p that was seen in the first part of the experiment was not seen when exposed to chromium after 24 hours. The anode showed a progressive but slow degradation throughout the 500 hours that showed a metastability after 144 hours at $R_P \cong\ 0.5\ \Omega cm^2$ which ended up being similar to the R_p that was measured on the last day of testing at $R_P \cong\ 0.6\ \Omega cm^2$. When looking at the SOFC Cathode side, the R_p stayed stable since the first day after polarization except for the data that was collected at 48 hours. The final R_p showed a similar value to the initial, being consistent throughout multiple sample tests. The overall R_p did not show any damage caused by the exposure to chromium. The effect of chromium on R_p will be analyzed in the following subsections through the Deconvolution of Distribution of Relaxation times.

4.3- SEM FIGURES

The SEM figures of both electrodes can give some insight as to why there are many differences between both functions and operating conditions.

The SEM figures of the electrodes under clean air conditions clearly reflect the way the current affects the electrode. There is one aspect that stands out when looking at the SOEC Anode side, and that is the interface. It can be seen how the closest layer of the electrode has bonded with the electrolyte much better than before operation. The current also impacted the grain size and the bonding between them. Those two factors could explain the reason behind the decrease in polarization resistance. Less pores were observed which could have hurt the gas diffusion mechanism, but it was not seen when looking at the DRT plots. The SOFC Cathode saw how the bonding at the electrode-electrolyte interface looked better, but the reduction in both the size and the number of pores could have been the main reason behind the increase in resistance polarization. Something that must be noted too is the difference in the structure of the electrode after polarization. The SOEC Anode seemed to be more fragile when analyzing the cross-section, whereas the SOFC Cathode structure seemed to not have suffered at all. The SOFC Cathode seemed to have a better organized microstructure than that of the SOEC Anode.

Although the structure seemed to be more organized than that of the sample running under clean-air conditions, the chromium particles have definitely damaged some of the processes within ORR and OER, mainly dissociative adsorption and its antagonist process and the surface diffusion mechanism. It seems like the exposure to chromium did not let the layers improve bonding as much as they did without any chromium. However, the SOFC Cathode seemed to have been more resilient towards chromium. The effect of polarization in microstructural changes was far less significant under the exposure to chromium. More pores are seen in the samples that ran under poisoned air, and therefore more diffusion channels for the oxygen molecules to flow through, which could end up being the explanation for the different behavior of the SOFC Cathode under both operating conditions.

4.4- DRT DECONVOLUTION

As stated before, the peak deconvolution of the Distribution of Relaxation Times gave a better insight as to what steps are the ones that account for the most part of the R_P. In section 3.7, DRT plots show the performance of both electrodes at different points under different external conditions such as temperature, pressure, and chromium exposure. These peaks are

plotted and distributed along the plot's x-axis depending on the frequency at which the process was plotted when performing the EIS analysis.

Each process is represented by one peak, although one peak could be hiding more than one process if these are happening at the same frequency. The main peaks are usually found from 10^3-10^1 hertz, tending to merge together in most of the plots. This fusing does not allow for an easy identification of the processes although the changes in resistance by changing external conditions can give some insight as to what peak can represent each of the processes. In order to find a better approximation of what the process could be, activation energies were found by collecting EIS analyses at different temperatures in the 700 ºC -800 ºC range. The activation energy of that process did not show a realistic activation energy value; therefore, it can be concluded that at least two processes are fusing together in that frequency range.

Both SOEC Anode and SOFC Cathode showed different responses to the chromium poisoning phenomenon. While SOEC Anode shows a progressive degradation throughout the 500 hours, the SOFC Cathode shows a more irregular progression throughout the experiment although it settled at the same level that it started the experiment at. This reflects the capacity of the SOFC Cathode to resist degradation when exposed to the chromium sources that were used in this experiment. When looking at the DRT plots, Peak 3 stands out as the main contributor to the overall resistance of each electrode apart from the SOEC Anode that was tested under clean air conditions. By comparing the changes that each of the processes went through under the presence of chromium once the experiment was finished, it can be seen how this peak is the one that suffers the most in the presence of chromium at the SOEC Anode side which leads to be the biggest difference in performance between both sides.

This peak could be identified as a surface process, as it goes through major resistance changes when exposed to different oxygen partial pressures. Other processes such as bulk diffusion would not show such a drastic difference when exposed to different oxygen concentrations in the atmosphere. This peak could correspond to the dissociative adsorption/ evolution reaction processes at SOFC Cathode and SOEC Anode respectively. The dissociative adsorption mechanism at the cathode side can be slowed down by chromium deposition on the surface, which would lead to a lower amount of oxygen adsorption onto

the surface, therefore concluding in a bigger resistance on consequent mechanisms but would not have resulted in a bigger resistance of the process. On the other hand, the oxygen evolution reaction would need a clear path for the oxygen ions to evolve into oxygen molecules on the electrode's surface. If these paths were to be blocked by chromium deposition, they would not be able to be released, creating an increasing buildup at the electrode surface that would translate into a linearly dependent degradation with time. This theory could explain and account for the difference in overall resistance between both sides at the end of the experiment.

5. CONCLUSION

The electrochemical behavior and performance of Ruddlesden-Popper phase Lanthanum Nickelate as air electrode for Reversible Solid Oxide Cells was analyzed through different techniques such as EIS, SEM, and DRT. The central part of the experiment was to establish how stable would the performance of LNO be in both modes, as SOEC Anode and SOFC Cathode.

The SOEC Anode data revealed that LNO is stable under clean air conditions and does not degrade throughout the 500 hours. When exposed to chromium, LNO seems to suffer more than under clean air conditions, although stability was reached halfway through the experiment. The R_p increases progressively until the end of the experiment from 0.18 to 0.6 Ωcm^2. The SOFC Cathode data seemed to represent an opposite behavior to that of the SOEC Anode. The SOFC Cathode showed a progressive degradation under clean-air conditions, increasing from 0.5 to 0.8 Ωcm^2. Under chromium exposure, the SOFC Cathode showed similar values at 0.3 Ωcm^2 at the beginning and the end of the experiment, showing a prospective excellent behavior under MIEC, especially when compared to other state-of-the-art materials such as LSM or LSCF.

On the topic of DRT understanding, more research needs to be performed to deeply understand the reason behind the difference between opposite electrodes in order to understand the differences in long-term performance. Understanding the difference in electrode surface behaviors of both electrodes could be key to achieving an optimal performance for R-SOCs.

6. BIBLIOGRAPHY

1. Amow, G., and S. J. Skinner. “Recent Developments in Ruddlesden–Popper Nickelate Systems for Solid Oxide Fuel Cell Cathodes.” *Journal of Solid State Electrochemistry* 10, no. 8 (April 22, 2006): 538–46. https://doi.org/10.1007/s10008-006-0127-x.
2. Banner, Jane, Ayesha Akter, Ruofan Wang, John Pietras, Soumitra Sulekar, Olga A. Marina, and Srikanth Gopalan. “Rare Earth Nickelate Electrodes Containing Heavily Doped Ceria for Reversible Solid Oxide Fuel Cells.” *Journal of Power Sources* 507 (September 2021): 230248. https://doi.org/10.1016/j.jpowsour.2021.230248.
3. Bentzen, J. J., J. V. T. HÃ¸gh, R. Barfod, and A. Hagen. “Chromium Poisoning of LSM/YSZ and LSCF/CGO Composite Cathodes.” *Fuel Cells* 9, no. 6 (December 2009): 823–32. https://doi.org/10.1002/fuce.200800143.
4. Biswas, Saheli, Shambhu Rathore, Aniruddha Kulkarni, Sarbjit Giddey, and Sankar Bhattacharya. “A Theoretical Study on Reversible Solid Oxide Cells as Key Enablers of Cyclic Conversion between Electrical Energy and Fuel.” *Energies* 14, no. 15 (July 26, 2021): 4517. https://doi.org/10.3390/en14154517.
5. Čebašek, Nebojša, Truls Norby, and Zuoan Li. “Kinetic Decomposition of a $La_2NiO_{4+\delta}$Membrane under an Oxygen Potential Gradient.” *Journal of the Electrochemical Society* 159, no. 8 (2012): F461–67. https://doi.org/10.1149/2.055208jes.
6. Cetin, Deniz, Sophie Poizeau, John Pietras, and Srikanth Gopalan. “Decomposition of La2NiO4 in Sm0.2Ce0.8O2-La2NiO4 Composites for Solid Oxide Fuel Cell Applications.” *Solid State Ionics* 300 (February 2017): 91–96. https://doi.org/10.1016/j.ssi.2016.11.030.
7. Choi, Sung Ryul, John-In Lee, Hyunyoung Park, Sung Won Lee, Dong Yeong Kim, Won Young An, Jung Hyun Kim, Jongsoon Kim, Hyun-Seok Cho, and Jun-Young Park. “Multiple Perovskite Layered Lanthanum Nickelate Ruddlesden-Popper Systems as Highly Active Bifunctional Oxygen Catalysts.” *Chemical Engineering Journal* 409 (April 2021): 128226. https://doi.org/10.1016/j.cej.2020.128226.

8. Coutanceau, Christophe, Stève Baranton, and Thomas Audichon. “Hydrogen Production from Water Electrolysis.” *Hydrogen Electrochemical Production*, 2018, 17–62. https://doi.org/10.1016/b978-0-12-811250-2.00003-0.
9. Gong, Yiwen, Ruofan Wang, Jane Banner, Soumendra N. Basu, Uday B. Pal, anSrikanth Gopalan. “Improved Tolerance of Lanthanum Nickelate (La2NiO4+δ) Cathodes to Chromium Poisoning under Current Load in Solid Oxide Fuel Cells.” *JOM* 71, no. 11 (August 20, 2019): 3848–58. https://doi.org/10.1007/s11837-019-03724-0.
10. Hou, Bingxue, Cheng Cheng Wang, Xumei Cui, and Yungui Chen. “Chromium Deposition and Poisoning of La $_2$ NiO $_4$ Cathode of Solid Oxide Fuel Cell.” *Royal Society Open Science* 5, no. 10 (October 2018): 180634. https://doi.org/10.1098/rsos.180634.
11. Ivers-Tiffée, E., A. Weber, and H. Schichlein. “O2-Reduction at High Temperatures: SOFC.” Handbook of Fuel Cells, December 15, 2010. https://doi.org/10.1002/9780470974001.f205045.
12. Jiang, San Ping. “Development of Lanthanum Strontium Cobalt Ferrite Perovskite Electrodes of Solid Oxide Fuel Cells – a Review.” International Journal of Hydrogen Energy 44, no. 14 (March 15, 2019): 7448–93. https://doi.org/10.1016/j.ijhydene.2019.01.212.
13. Laberty, Christel, Feng Zhao, Karen E. Swider-Lyons, and Anil V. Virkar. “High-Performance Solid Oxide Fuel Cell Cathodes with Lanthanum-Nickelate-Based Composites.” Electrochemical and Solid-State Letters 10, no. 10 (2007): B170. https://doi.org/10.1149/1.2760188.
14. Lee, Younki, and Haekyoung Kim. “Electrochemical Performance of La2NiO4+δ Cathode for Intermediate-Temperature Solid Oxide Fuel Cells.” Ceramics International 41, no. 4 (May 2015): 5984–91. https://doi.org/10.1016/j.ceramint.2015.01.037.
15. Lyagaeva, Yu. G., N. A. Danilov, M. Yu. Gorshkov, G. K. Vdovin, B. D. Antonov, A. K. Demin, and D. A. Medvedev. “Functionality of Lanthanum, Neodymium, and Praseodymium Nickelates as Promising Electrode Systems for

Proton-Conducting Electrolytes." Russian Journal of Applied Chemistry 91, no. 4 (April 2018): 583–90. https://doi.org/10.1134/s1070427218040080.

16. Maas, Klaasjan. "La2NiO4+D, a Mixed Ionic-Electronic Conductor for Interface-Type Valence Change Memories." theses.hal.science, March 14, 2019. https://theses.hal.science/tel-02160021/.
17. Majewski, Artur J., Anna Khodimchuk, Dmitriy Zakharov, Natalia Porotnikova, Maxim Ananyev, Ian D. Johnson, Jawwad A. Darr, Peter R. Slater, and Robert Steinberger-Wilckens. "Oxygen Surface Exchange Properties and Electrochemical Activity of Lanthanum Nickelates." Journal of Solid State Chemistry 312 (August 2022): 123228. https://doi.org/10.1016/j.jssc.2022.123228.
18. Montenegro-Hernández, Alejandra, Jesús Vega-Castillo, Liliana Mogni, and Alberto Caneiro. "Thermal Stability of Ln2NiO4+δ (Ln: La, Pr, Nd) and Their Chemical Compatibility with YSZ and CGO Solid Electrolytes." International Journal of Hydrogen Energy 36, no. 24 (December 1, 2011): 15704–14. https://doi.org/10.1016/j.ijhydene.2011.08.105.
19. Nezhad, Parastoo Delir Kheyrollahi, Maged F. Bekheet, Nicolas Bonmassar, Lukas Schlicker, Albert Gili, Franz Kamutzki, Aleksander Gurlo, et al. "Mechanistic in Situ Insights into the Formation, Structural and Catalytic Aspects of the La2NiO4 Intermediate Phase in the Dry Reforming of Methane over Ni-Based Perovskite Catalysts." Applied Catalysis A: General 612 (February 2021): 117984. https://doi.org/10.1016/j.apcata.2020.117984.
20. Nirala, Gurudeo, Dharmendra Yadav, and Shail Upadhyay. "Ruddlesden-Popper Phase A2BO4 Oxides: Recent Studies on Structure, Electrical, Dielectric, and Optical Properties." Journal of Advanced Ceramics 9, no. 2 (March 26, 2020): 129–48. https://doi.org/10.1007/s40145-020-0365-x.
21. O'Hayre, Ryan P., Suk-Won Cha, Whitney G. Colella, and F. B. Prinz. Fuel Cell Fundamentals. Hoboken, New Jersey: John Wiley & Sons Inc., 2016.
22. Pandiyan, Arunkumar, Aarthi Uthayakumar, Rengaraj Subrayan, Suk Won Cha, and Suresh Babu Krishna Moorthy. "Review of Solid Oxide Electrolysis Cells: A

Clean Energy Strategy for Hydrogen Generation." Nanomaterials and Energy 8, no. 1 (June 2019): 2–22. https://doi.org/10.1680/jnaen.18.00009.

23. Pikalova, E., N. Bogdanovich, A. Kolchugin, L. Ermakova, A. Khrustov, A. Farlenkov, and D. Bronin. "Methods to Increase Electrochemical Activity of Lanthanum Nickelate-Ferrite Electrodes for Intermediate and Low Temperature SOFCs." International Journal of Hydrogen Energy 46, no. 72 (October 2021): 35923–37. https://doi.org/10.1016/j.ijhydene.2021.01.226.
24. Pikalova, Elena, Alexander Kolchugin, Kiryl Zakharchuk, Dziyana Boiba, Viktor Tsvinkinberg, Elena Filonova, Anton Khrustov, and Aleksey Yaremchenko. "Mixed Ionic-Electronic Conductivity, Phase Stability and Electrochemical Activity of Gd-Substituted La2NiO4+δ as Oxygen Electrode Material for Solid Oxide Fuel/Electrolysis Cells." International Journal of Hydrogen Energy 46, no. 32 (May 2021): 16932–46. https://doi.org/10.1016/j.ijhydene.2021.03.007.
25. Sayers, R., M. Rieu, P. Lenormand, F. Ansart, J.A. Kilner, and S.J. Skinner. "Development of Lanthanum Nickelate as a Cathode for Use in Intermediate Temperature Solid Oxide Fuel Cells." Solid State Ionics 192, no. 1 (June 2011): 531–34. https://doi.org/10.1016/j.ssi.2010.02.014.
26. Schrödl, N., A. Egger, C. Gspan, T. Höschen, F. Hofer, and W. Sitte. "Phase Decomposition of La2NiO4+δ under Cr- and Si-Poisoning Conditions." Solid State Ionics 322 (September 2018): 44–53. https://doi.org/10.1016/j.ssi.2018.05.002.
27. Tian, Hanchen, Wenyuan Li, Liang Ma, Tao Yang, Bo Guan, Wangying Shi, Thomas L. Kalapos, and Xingbo Liu. "Deconvolution of Water-Splitting on the Triple-Conducting Ruddlesden-Popper-Phase Anode for Protonic Ceramic Electrolysis Cells." ACS Applied Materials & Interfaces 12, no. 44 (November 4, 2020): 49574–85. https://doi.org/10.1021/acsami.0c12987.
28. Tse, Edmund C. M., and Andrew A. Gewirth. "Effect of Temperature and Pressure on the Kinetics of the Oxygen Reduction Reaction." The Journal of Physical Chemistry A 119, no. 8 (February 16, 2015): 1246–55. https://doi.org/10.1021/acs.jpca.5b00572.

29. Wang, Ruofan, Zhihao Sun, Yanchen Lu, Srikanth Gopalan, Soumendra N. Basu, and Uday B. Pal. “Comparison of Chromium Poisoning between Lanthanum Strontium Manganite and Lanthanum Strontium Ferrite Composite Cathodes in Solid Oxide Fuel Cells.” Journal of Power Sources 476 (November 2020): 228743. https://doi.org/10.1016/j.jpowsour.2020.228743.
30. Wu, Ji, Stevin S. Pramana, Stephen J. Skinner, John A. Kilner, and Andrew P. Horsfield. “Why Ni Is Absent from the Surface of La2NiO4+δ?” Journal of Materials Chemistry A 3, no. 47 (2015): 23760–67. https://doi.org/10.1039/c5ta03759j.
31. Yasuda, K, K Uemura, and T Shiota. “Sintering and Mechanical Properties of Gadolinium-Doped Ceria Ceramics.” Journal of Physics: Conference Series 339, no. 1 (January 31, 2012): 012006. https://doi.org/10.1088/1742-6596/339/1/012006.
32. Yin, Baoyi, Yining Li, Ningqiang Sun, Xiaohui Ji, Yu Huan, Dehua Dong, Xun Hu, and Tao Wei. “Activating ORR and OER in Ruddlesden-Popper Based Catalysts by Enhancing Interstitial Oxygen and Lattice Oxygen Redox Reactions.” Electrochimica Acta 370 (February 2021): 137747. https://doi.org/10.1016/j.electacta.2021.137747.
33. Yoo, Young-Sung, Mihwa Choi, Jin-Ha Hwang, Ha-Ni Im, Bhupendra Singh, and Sun-Ju Song. “La2NiO4+δ as Oxygen Electrode in Reversible Solid Oxide Cells.” Ceramics International 41, no. 5 (June 2015): 6448–54. https://doi.org/10.1016/j.ceramint.2015.01.083.
34. Zhou, Lingfeng, Jerry H. Mason, Wenyuan Li, and Xingbo Liu. “Comprehensive Review of Chromium Deposition and Poisoning of Solid Oxide Fuel Cells (SOFCs) Cathode Materials.” Renewable and Sustainable Energy Reviews 134 (December 2020): 110320. https://doi.org/10.1016/j.rser.2020.110320.
35. Zhu, Wei-zhong, and Mi Yan. “Perspectives on the Metallic Interconnects for Solid Oxide Fuel Cells.” Journal of Zhejiang University-SCIENCE A 5, no. 12 (December 2004): 1471–1503. https://doi.org/10.1631/jzus.2004.1471.
36. Zhu, Zhikuan, Michelle Sugimoto, Uday Pal, Srikanth Gopalan, and Soumendra Basu. “Electrochemical Cleaning: An In-Situ Method to Reverse Chromium

Poisoning in Solid Oxide Fuel Cell Cathodes." Journal of Power Sources 471 (September 2020): 228474. https://doi.org/10.1016/j.jpowsour.2020.228474.

37. Vibhu, Vaibhav, Aurélien Flura, Aline Rougier, Clément Nicollet, Sébastien Fourcade, Teresa Hungria, Jean-Claude Grenier, and Jean-Marc Bassat. "Electrochemical Ageing Study of Mixed Lanthanum/Praseodymium Nickelates La2-Pr NiO4+δ as Oxygen Electrodes for Solid Oxide Fuel or Electrolysis Cells." *Journal of Energy Chemistry* 46 (July 2020): 62–70. https://doi.org/10.1016/j.jechem.2019.10.012.
38. Mercy, Alain, Jordan Bieder, Jorge Íñiguez, and Philippe Ghosez. 2017. "Structurally Triggered Metal-Insulator Transition in Rare-Earth Nickelates." *Nature Communications* 8 (1). https://doi.org/10.1038/s41467-017-01811-x.
39. Nikonov, A.V., et al. "A Brief Review of Conductivity and Thermal Expansion of Perovskite-Related Oxides for SOFC Cathode." Eurasian Journal of Physics and Functional Materials, vol. 2, no. 3, 26 Sept. 2018, pp. 274–292, https://doi.org/10.29317/ejpfm.2018020309. Accessed 23 Nov. 2021.
40. "Hydrogen Economy and Fuel Cell Technology Research." *Vaisala*, www.vaisala.com/en/blog/2022-12/hydrogen-economy-and-fuel-cell-technology-research. Accessed 12 Apr. 2023.
41. "Two,Three,Four Electrode System Gamry 4-Probe Potentiostats." n.d. Www.gamry.com. https://www.gamry.com/application-notes/instrumentation/two-three-four-electrode-experiments/.
42. "Solid Oxide Based Electrolysis and Stack Technology with Ultra-High Electrolysis Current Density and Efficiency." 2015. https://www.hydrogen.energy.gov/pdfs/review15/pd124_petri_2015_p.pdf.